

Magnetostatic Spin Waves and Magnetic-Wave Chaos in Ferromagnetic Films.

III. Numeric Simulations of Microwave-Band Magnetic Chaos, Its Synchronization and Application to Secure Communication

A.A. Glushchenko, Yu.E. Kuzovlev, Yu.V. Medvedev, and N.I. Mezin*

A.A.Galkin Physics and Technology Institute of NASU,

ul. R.Luxemburg 72, 83114 Donetsk, Ukraine

Abstract

Selected results of original numeric simulations of non-linear magnetostatic spin waves and microwave-frequency magnetic chaos in ferrite films are expounded, as third part of the work whose first two parts are recent arXiv preprints 1204.0200 and 1204.2423 . Especially we consider crucial role of parametric processes in creating the chaos and simultaneously obstacles to its synchronization, and examine some possibilities of good enough synchronization (to an extent allowing its use for direct secure communication in microwave band).

PACS numbers: 75.30.Ds, 75.40.Mg, 76.50.+g

*Electronic address: kuzovlev@fti.dn.ua

Introduction

This preprint continues preprints 1204.0200 and 1204.2423 and represents some results of numerical simulations of auto-generation magnetic-wave chaos in ferrite films, its synchronization and application to secure communication. A references like (6.x) means formula (x) from Section 6 placed in 1204.2423. Sections 1-5 are placed in 1204.0200.

Our main interest below is

(i) visual investigation of regular and chaotic non-linear magnetostatic spin wave patterns auto-generated through feedback consisting of wire inductors (antennae), amplifier and may be filters;

(ii) investigation of those conditions of the auto-generation, and properties of generated patterns, what are mostly responsible for characteristics of resulting chaotic microwave-band electric signals (voltages and currents), in particular, their possibilities to synchronize chaotic patterns in other similar systems (ferrite film) and thus to serve for secure transmission of information.

7. NUMERIC SIMULATIONS OF AUTO-GENERATION AND SYNCHRONIZATION OF MAGNETIC-WAVE CHAOS

7.1. CHAOTIC AUTO-GENERATION IN FILM WITH LINEAR FEEDBACK.

If the voltage (EMF) signal, $U(t)$, induced in a conductor (antenna) by magnetization precession is amplified and transformed into driving current, $J(t)$, in another conductor, then auto-generation of MW may take place. The simplest variant of this feedback is drawn at plot (A) in Fig.13. It consists of two identical loop inductors and purely linear amplifier whose gain and phase shift are with frequency independent. Typical features of chaotic generation in such the scheme, at $H_0 = 2$, are presented by Figs.13 and 14.

The plots (B) and (E) in Fig.13 show that rather wide-band magnetization chaos is produced, in frequency range about 600 MHz. Position of most intensive peak at the voltage spectrum well corresponds to frequency of the Damon-Eshbach (DE) surface wave with length $\lambda = 2l = 32D$ dictated by the loop width, i.e. to $\omega_{DE} = \omega_{DE}(2\pi D/\lambda)$ (≈ 2.54 GHz at $H_0 = 2$). The lower edge of the spectrum lies below uniform precession frequency ω_u (≈ 2.12 GHz). This means that the main-branch bulk waves also are

excited. The upper edge of the voltage spectrum is far below the upper frequency of MSW, $(H_0 + 2\pi)f_0$ (≈ 3.25 GHz). Hence, long surface MSW are dominating in magnetization patterns.

This pattern is seen at plot (A) in Fig.14. The contour plot of its spatial spectrum ((F) in Fig.14) demonstrates tracks of (i) a set of long-wave modes with frequencies about ω_u , (ii) three times shorter than λ DE mode with frequency $\omega_{DE}(3 \cdot 2\pi D/\lambda)$ (≈ 2.95 GHz), (iii) comparatively short-wave surface modes with non-zero transversal wavenumber, $k_y \neq 0$, and frequencies about $\omega_{DE}(2\pi D/\lambda)$, and, besides, (iv) approximately two times longer than λ DE mode with frequency $\approx \omega_{DE}(\pi D/\lambda)$ (≈ 2.36 GHz).

Interestingly, the latter mode seems be responsible for lower high peak in the voltage spectrum. Plots (B) and (C) show that, in rough terms, auto-generation switches between two states whose frequencies are about $\omega_{DE}(2\pi D/\lambda)$ and $\omega_{DE}(\pi D/\lambda)$, and that at the first of them the energy is usually lower than at the second (in accordance with negative non-isochronity, see Sec.5).

Due to linearity of amplifier, the film itself are forced to take all cares about nonlinear saturation of precession angle. Naturally, this results in complicated large-amplitude chaos characterized by wide variety of time scales and intermittency of different regimes, which is illustrated by plots (B)-(D) in Fig.13 and (B),(C) and (E) in Fig.14. Low-frequency contents of this chaos is better visible in the spectrum of energy, $E(t)$, which is enriching at least down to 5 MHz. Voltage and magnetization time series yield fractal dimension $d_{cor} \approx 3.45$. Hence, we encounter hyper-chaos governed by not less than four relevant variables.

7.2. AUTO-GENERATOR WITH NON-LINEAR FEEDBACK.

As practice says, in real generators an inner non-linearity of amplifiers is essential. It manifests itself in two ways: (i) as non-linearity of input resistance which effectively saturates input voltage, and (ii) as saturation of output power or, equivalently, of output driving current. Besides, one should take into account frequency dependence of gain, $K(\omega)$, and own impedances (capacities and inductances) of feedback conductors.

Corresponding scheme looks as in Fig.15. Here R_0 , L_0 and C_0 are linear (small-amplitude) input resistance, ~ 50 Ohm, inductance of passive (feedback) antenna, ~ 5 nH, and capacity of active (driving) antenna, ~ 0.5 pF, respectively. Since in reality such the circuit is quasi-stationary one (its size is much smaller than lengths of EM-waves under operation), a simple analysis shows that there is no necessity in additional reactive elements.

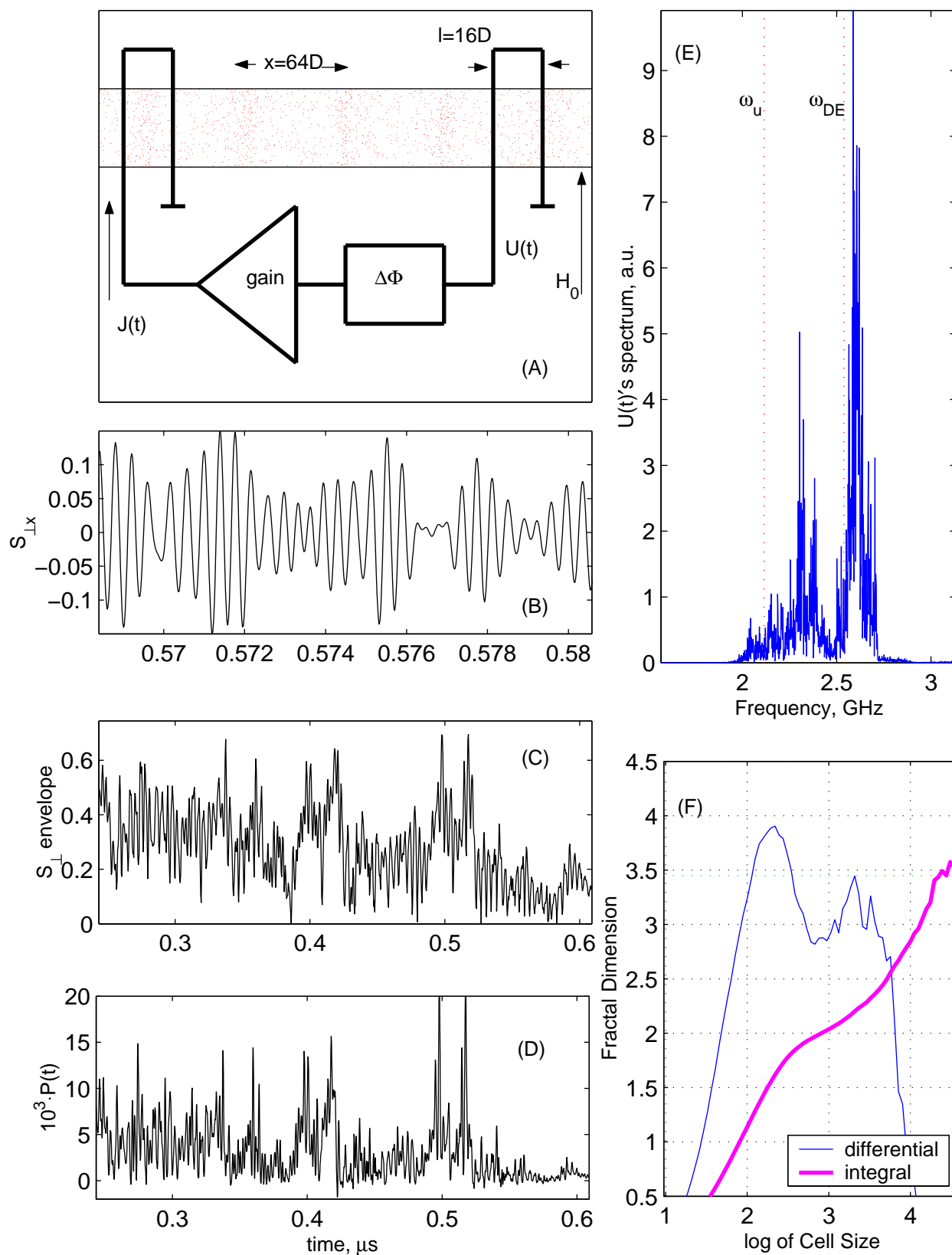


Fig.13. Chaotic auto-generation in tangentially magnetized film closed on itself by two loop inductors and linear amplifier with frequency-independent gain and phase shift, $\Delta\Phi$, at $H_0=2M_s$. (A) Passive loop is the source of voltage, $U(t)$, proportional to $dS_{\perp x}/dt$. The current, $J(t)$, of active loop excites spin precession. (B) $S_{\perp x}$ in vicinity of passive loop. (C) $S_{\perp x}$'s envelope. (D) Power absorption. (E) Spectrum of $S_{\perp x}$. (F) Correlation dimension of $U(t)$ and $S_{\perp x}$ occurs $d_{\text{cor}} \approx 3.45$.

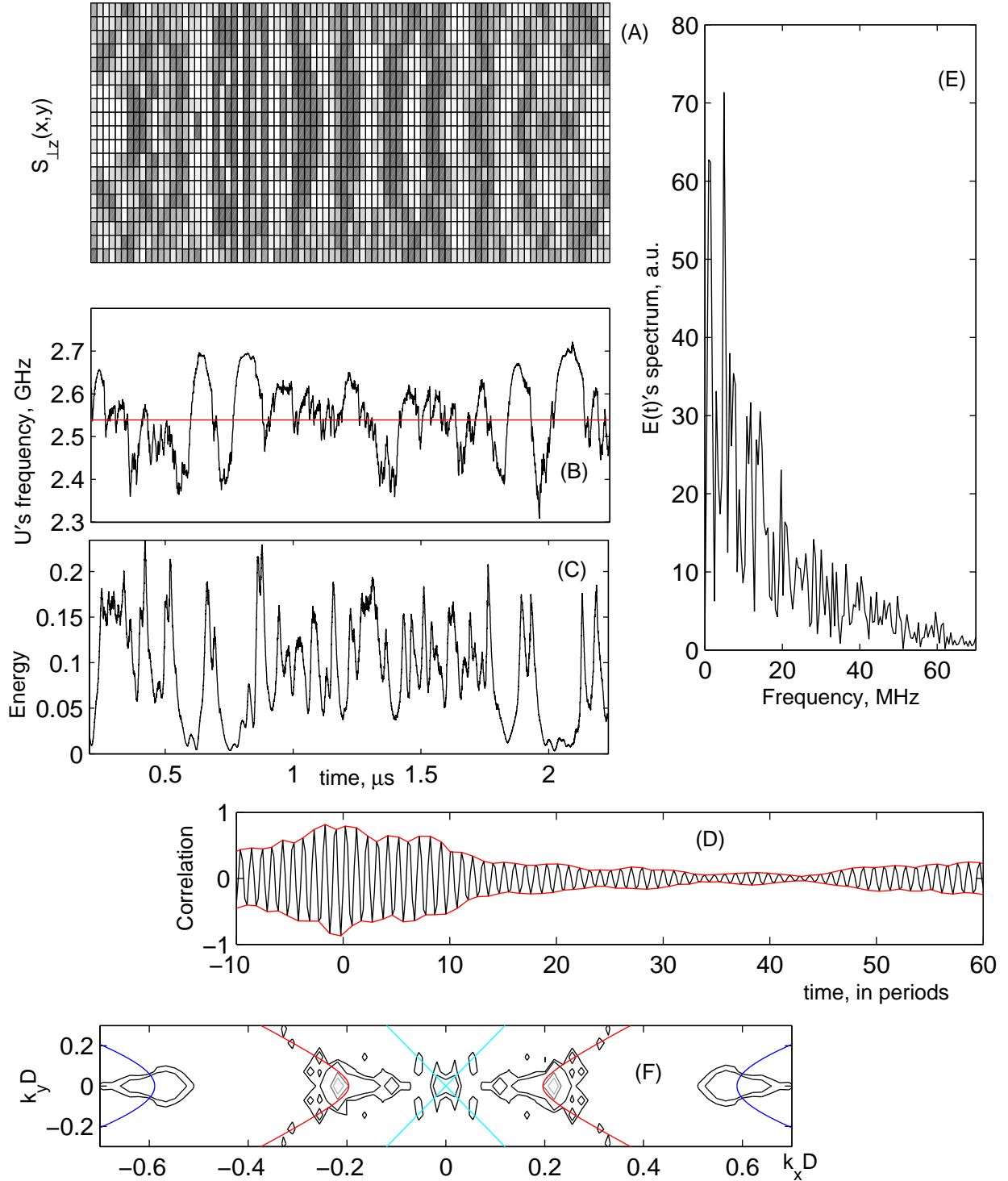


Fig.14. Chaotic MSW auto-generation (continued from Fig.13). (A) Typical S_{\perp} pattern. (B) Instant voltage frequency, $\omega_{in}(t)$, obtained from its zero crossings. Strict line shows the surface MSW frequency, $\omega_{DE}(kD)$, which corresponds to $k_x=2\pi/\lambda$ (at $k_y=0$), with $\lambda=2l=32D$ being wavelength selected by the loop geometry (see Fig.13(A)). (C) Excess energy, $E(t)$. Negative correlation between $E(t)$ and $\omega_{in}(t)$ is clearly seen. (D) Mutual correlation of magnetizations, S_{\perp} , about active and passive loops. (E) Energy spectrum. (F) Contour plot of S_{\perp} . Three equi-frequency lines are shown corresponding to surface MSW in infinite-size film with frequencies ω_u (uniform precession), $\omega_{DE}(2\pi D/\lambda)$ and $\omega_{DE}(3\cdot 2\pi D/\lambda)$.

For practical high-frequency wide-band amplifiers, typical level of the input saturation is $U_{sat} \sim 1 \div 3$ V, level of output saturation is $J_{sat} \sim 20 \div 70$ mA, while $K_0 = \max |K(\omega)| \sim 5 \div 15$, and linear frequency characteristics can be modeled by

$$K(\omega) = K_0 \omega_0^2 (\omega_0^2 - \omega^2 - ig\omega)^{-1} \exp(i\omega\tau_d) , \quad (1)$$

with τ_d describing time delay. In numerical simulations, usually values $\omega_0/2\pi = 3.4$ GHz and $g = 6 \cdot 10^9$ s⁻¹ were used, as in INA-32063 wideband silicon RFIC amplifier (τ_d is small as compared with time delays in film and therefore insignificant).

Fig.15 shows how numerical copy of this scheme generates at relatively small gain, $K_0 \approx 5$, and moderate output power saturation. We see that likely periodic (although more or less complicated) oscillations take place in all the amplitudes and phases. If decreasing gain and /or output saturation level one may observe more simple oscillations, down to trivial mono-chromatic regime and failure of generation, while increase results in further complications and then chaos.

7.3. ROLE OF ANTENNAE SEPARATION.

The Fig.16 illustrates chaotic auto-generation in numerical model corresponding to 4.4 mm \times 0.9 mm \times 10 μ m-size film and $l = 0.5$ mm width of loop inductors, or to a proportionally re-scaled system (but not too small), at field $H_0 = 500$ Oe, moderate gain and relatively high output power saturation. At top of Fig.16 static magnetization of such shaped film, at $M_s = 140$ Oe and $H_0 = 500$ Oe, is presented. Clearly, a noticeable demagnetization takes place at film corners only.

In this numerical experiment, two variants of separation, x , of feedback and active inductors were considered, with $x = x_1 = 2\lambda$ and $x = x_2 = 1.8\lambda$, where $\lambda = 2l = 1$ mm is maximum of wavelengths preferably selected by the loop antennae. Comparison of these cases demonstrates, at plot (D), that auto-generation spectrum is sensitive not only to the λ but also to x . It could be expected, because any phase shift in feedback should be compensated by equal magnetic wave phase difference, $k_x x$, between antennae, with k being a dominating wave vector. At smooth feedback frequency characteristics, one can suppose that $k_{1x} x_1 \approx k_{2x} x_2$, therefore

$$k_{2x} - k_{1x} \approx -k_{1x}(x_2 - x_1)/x_1, \quad \omega_2 - \omega_1 \approx v_g(k_{2x} - k_{1x}), \quad (2)$$

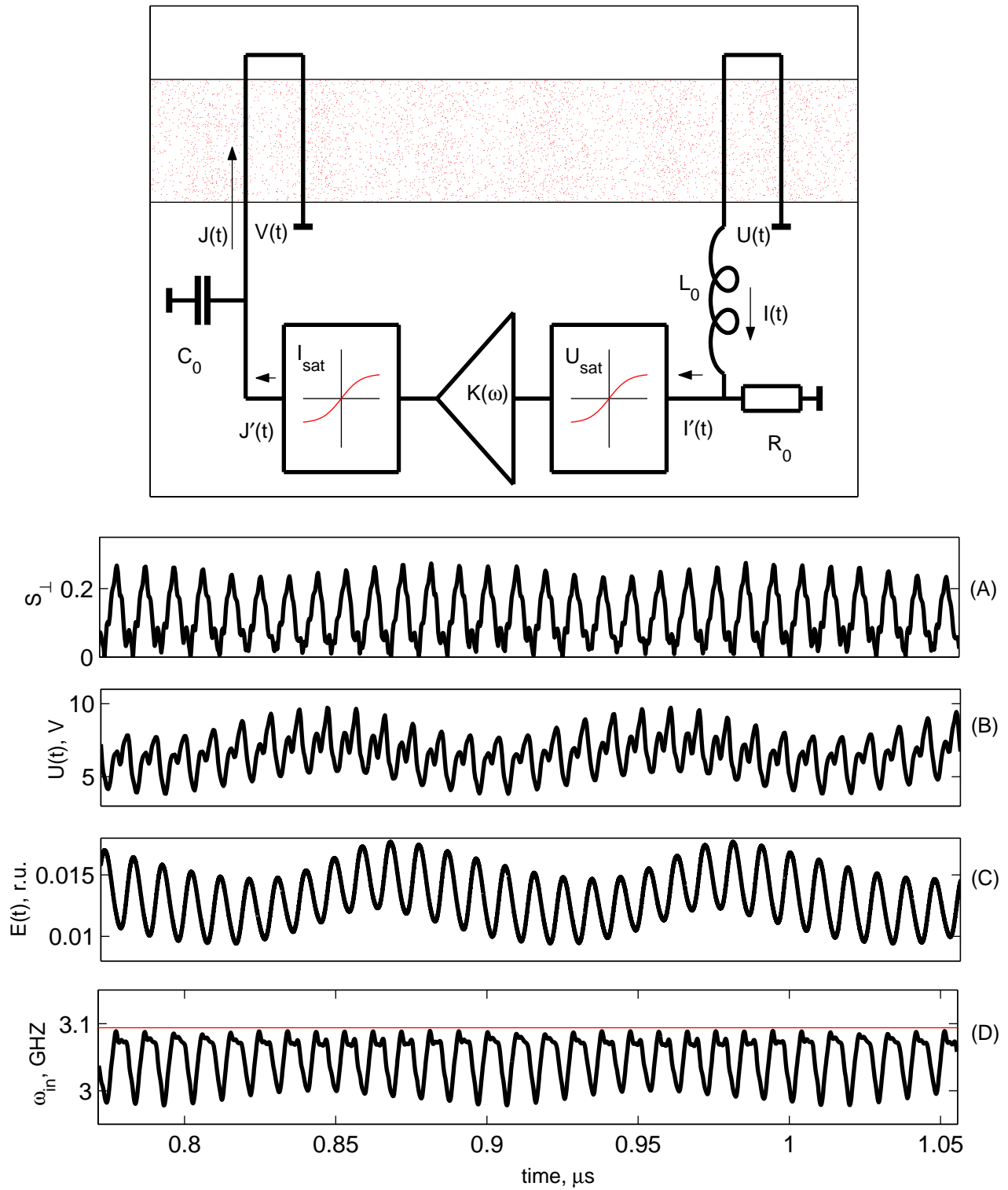


Fig.15. (Top) Principal scheme of auto-generator under numerical simulation. (Below) Regular auto-oscillations at the parameters as follows: $H_0=500$ Oe, $\gamma=0.0007$, $R_0=50$ Ohm, $C_0=0.5$ pF, $L_0=5$ nH, $U_{sat}=1$ V, $I_{sat}=40$ mA, $d=10\mu$, $\lambda=0.1$ cm, $x=2\lambda$. (A) Envelope of x -component of spin precession, $S_{\perp x}$, about passive loop. (B) Envelope of voltage, $U(t)$. (C) Excess energy, $E(t)$. (D) Instant voltage frequency from zero crossings. Strict line shows frequency $\omega_{DE}(2\pi D/\lambda)$.

where $\omega_2 - \omega_1$ is corresponding change in frequency and v_g is group velocity. According to this estimate, transition from $x_1 = 2\lambda$ to $x_2 = 1.8\lambda$ must result in increase of auto-generation frequencies, which agrees with numerical simulation. Taking ω be the frequency of DE wave, we obtain $v_g \approx 4\pi^2 D/\omega_1$ and then $\omega_2 - \omega_1 \approx 0.032$ (in dimensionless units), that is ≈ 13 MHz, in satisfactory quantitative agreement with plot (D).

Let us more discuss the voltage spectrum. As in case of linear feedback (see above), its upper-frequency peak can be surely related to DE mode with $k_x \approx 2\pi/\lambda$. But what is origin of the lower-frequency peak? From watching for dynamics of magnetization pattern, it is possible to relate this peak to a long DE mode with wavelength nx where $1 \lesssim n \lesssim 2$. Such mode also can get suitable phase conditions under feedback determined by Eq.1.

7.4. HYPER-CHAOS UNDER NON-LINEAR FEEDBACK.

Non-linear concurrence between the two dominating wave modes manifests itself in chaotic jumps of instant (time-local) frequency of auto-generation, $\omega_{in}(t)$, as shown by plots (A) and (C) in Fig.16. It should be underlined that from the point of view of energy pattern (quasi-local energy, see Sec.6.14) the same interplay of different modes looks as the birth and drift of envelope solitons. In these terms, the frequency separation of two main peaks at plot (D) is nothing but mean number of soliton births per second (see below).

Due to high power saturation level, the whole picture occurs very chaotic. Its correlation dimension obtained from voltage and magnetization time series (solid and dot lines, respectively) is $d_{cor} \approx 4$ (if not greater).

7.5. WEAK CHAOS IN GENERATOR WITH WIRE INDUCTORS.

It is interesting how the picture will be changed if two-element loop inductors are replaced by wires, at the same feedback circuit. Figs.17a and 17b can give the answer for case $x = 150D$ ($=1.5$ mm) with x being distance between the wires.

In this case, two dominating modes chosen by the system are long DE waves with lengths $\approx 2x$ and $\approx x$. In spatial spectrum of magnetization (in momentum space) the mode with length $\approx x/2$ can be detected, but practically it does not contribute to voltage spectrum. Besides, as usually, a set of comparatively weak excited equal-frequency modes with $k_y \neq 0$ is present. In real space non-linear magnetization pattern characteristic rhombic structuring is well visible invoked by dispersing properties of underlying linear MW eigenmodes. But frequencies of the latter become lowered by non-linearity.

At nearly the same output saturation and even greater linear gain, the whole picture is

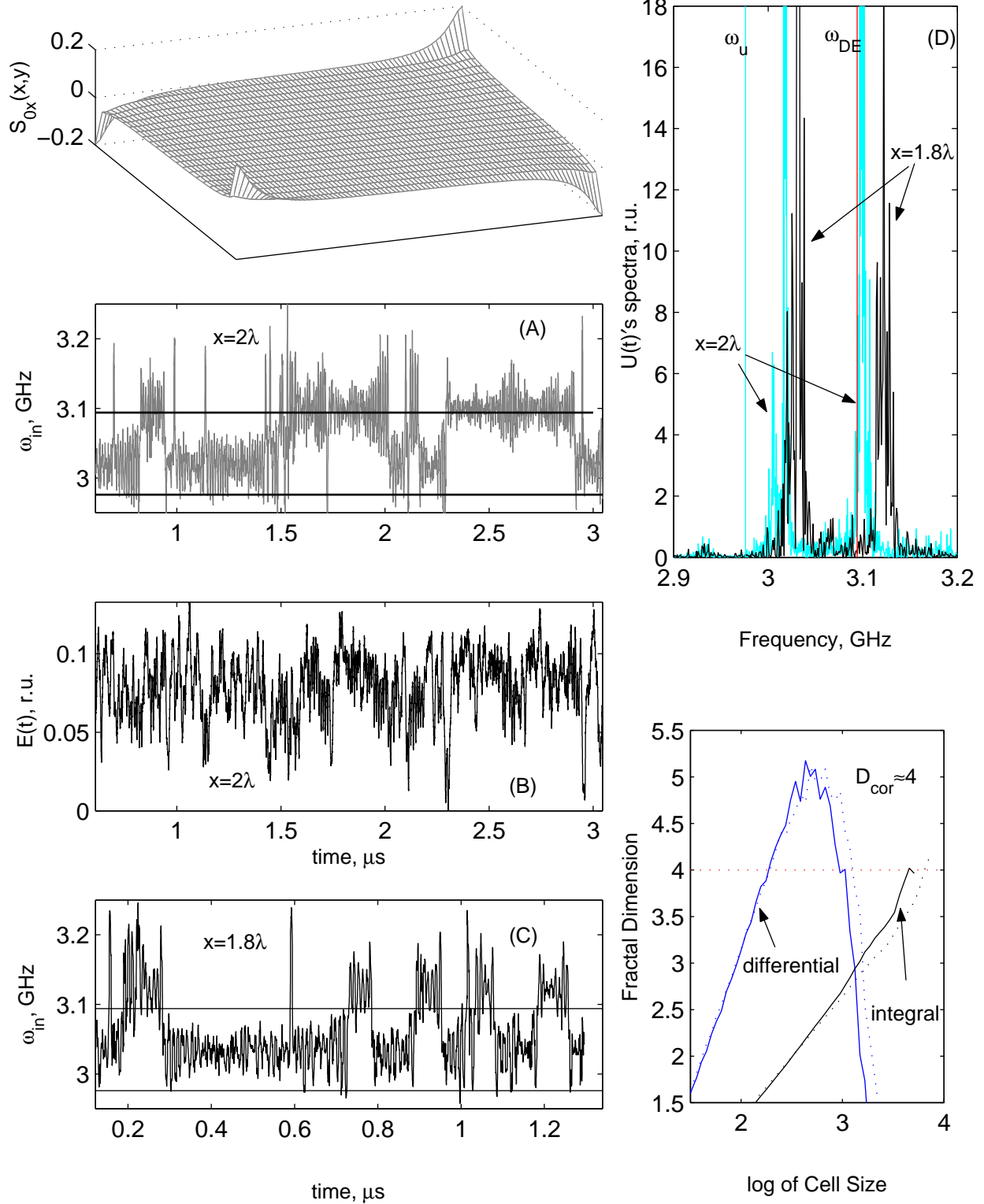


Fig.16. (Top left) x -component of static magnetization in relatively large-area 440D×90D film. (Other) Hyperchaos in two auto-generators, at $H_0=500$ Oe, $\gamma=0.0012$, $R_0=50$ Ohm, $C_0=0.5$ pF, $L_0=5$ nH, $U_{\text{sat}}=1$ V, $I_{\text{sat}}=70$ mA, Gain=7, $D=10\mu$, $\lambda=0.1$ cm. The only difference between the two is in inter-loop distance, $x=2\lambda$ and $x=1.8\lambda$. The smaller distance results in higher frequency. Direct lines in (A), (C) and (D) show uniform precession frequency, ω_u , and surface MSW frequency $\omega_{\text{DE}}(2\pi D/\lambda)$.

significantly more smooth and less chaotic than in case of loop inductors, with $d_{cor} \approx 2.55$ only! In part, the reason is that both the EMF accepted by wire inductor and power pumped by it are approximately two times smaller than by loop inductor. In this concrete experiment, power absorption $P \approx \langle JV \rangle_T \sim 25$ mW, where J and V are driving current and EMF in active inductor, respectively, and $\langle \dots \rangle_T$ means time average (over a few precession periods).

7.6. GENERATION OF ENVELOPE SOLITONS.

In the middle plot in Fig.17b, typical spatial distribution of the quasi-local energy density (Sec.6.14) is shown (to be precise, of e_{loc}/H_0 where H_0 is M_s units). It highlights presence of three envelope solitons of whose the first (most left) is in birth, the second is just passing through feedback inductor and the third is dying remainder of previously passed soliton. Obvious rhombic shaping of the solitons reflects four most preferred directions of local energy propagation (corresponding to maximum group velocity), $|v_{gy}|/|v_{gx}| \approx \sqrt{H_0/4\pi}$ (see Sec.5.4).

Notice that solitons are very sharp (as measured in x -direction): their width is even less than wavelengths of carry MSW enveloped by them! But several wavelengths have time to pass through such the envelope while it itself displaces on its width.

7.7. INSTANTON STRUCTURING OF SPIN PRECESSION.

Let us go back to strong chaos considered above in subsection 4 and have a look how envelope solitons manifest themselves in local magnetization time series. The Fig.18 shows behavior of spin and of e_{loc}/H_0 , where e_{loc} is quasi-local energy density (Sec.6.14), at a point close to the feedback inductor. Notice that

$$e_{loc}/H_0 \approx (S_x^2 + p^2 S_z^2)/2 \approx p|\Psi|^2/2, \quad (3)$$

where Ψ is the wave function (see in Sec.5.3 and Eq.5.9 there), and p is the eccentricity (see Eqs.4.6 and 5.10), i.e. can be interpreted as merely squared angle of precession. Comparison of plots (C) and (D) in Fig.18 visually prove that at fast time scale (measured in periods of precession) e_{loc} is almost integral of motion.

What most of all impresses in plots (B), (C) and (F) is that e_{loc} (and thus local angle of precession) never overlooks to regularly turn into either exact zero or to extremely small value. If $S_{\perp}(r, t)$ was mere random field (like thermally activated magnetization noise in thermodynamical equilibrium) such behavior would be absolutely improbable. It gives best

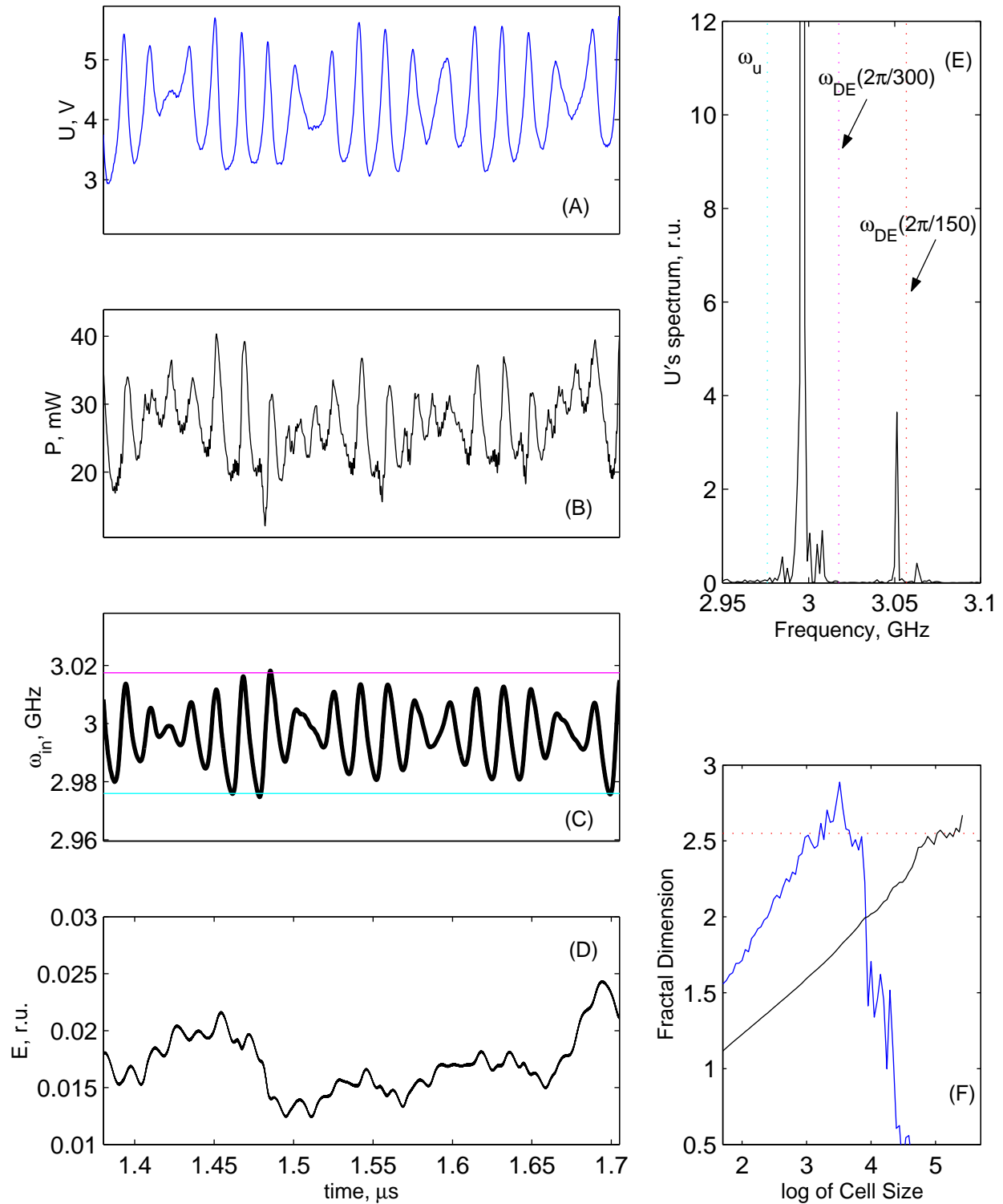


Fig.17a. Relatively slightly chaotic oscillations in auto-generator with two wire inductors instead of loop ones, at the parameters as follows: $H_0=500$ Oe, $\gamma=0.001$, $R_0=50$ Ohm, $C_0=0.5$ pF, $L_0=5$ nH, $U_{\text{sat}}=1$ V, $I_{\text{sat}}=60$ mA, Gain=10, $D=10\mu$. Separation of inductors equals to $x=150D=0.15$ cm. The primarily excited DE MSW mode has wave length $\lambda=2x$. (A) Envelope of voltage on passive inductor, $U(t)$. (B) Envelope of power absorption, $P(t)$. (C) Instant frequency from $U(t)$'s zero crossings. (D) Excess energy per unit volume. (E) Voltage spectrum. (F) Correlation dimension obtained from the voltage signal is $d_{\text{cor}} \approx 2.55$. Horizontal lines in (C) and dotted lines in (E) correspond to ω_u , $\omega_{\text{DE}}(2\pi D/\lambda)$ and $\omega_{\text{DE}}(4\pi D/\lambda)$, with $\lambda=2x=300D$. 11

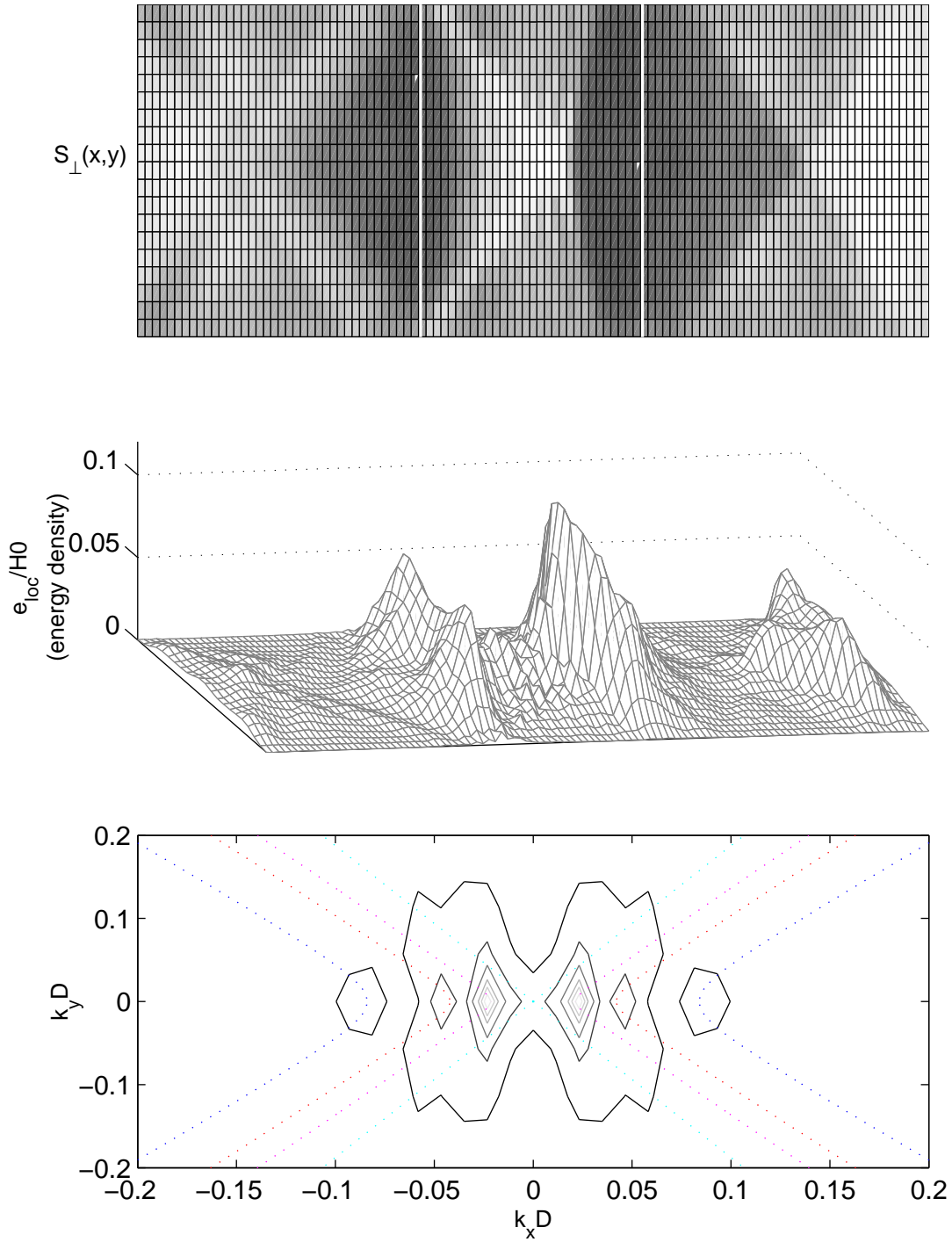


Fig.17b. Continuation to Fig.17a. (Top) Instant S_{\perp} pattern. Light lines show positions of the wire inductors. (Middle) Typical spatial distribution of $e_{\text{loc}}/H_0 = 1 - S_{\parallel} + 2\pi S_{\perp}^2/H_0$ with e_{loc} being quasi-local energy density (see main text). The presence of three narrow solitons is seen which possess characteristic rhombic shaping and the length on order of mean wavelength. (Bottom) Contour plot of spatial spectrum of S_{\perp} . The dotted curves are equi-frequency lines corresponding to ω_u , $\omega_{\text{DE}}(2\pi D/\lambda)$, $\omega_{\text{DE}}(4\pi D/\lambda)$ and $\omega_{\text{DE}}(8\pi D/\lambda)$, with $\lambda=2x$.

evidence that we observe results of essentially nonlinear self-organization of magnetization field in “clots”. As in nonlinear field theory, spatially local time tracks of self-organization may be termed instantons.

As it was mentioned in Sec.5.4, to be more precise, the eccentricity, p , should be related to dominating MSW mode (instead of uniform one). In other words, the quasi-local energy introduced in Eq.6.6 must be redefined with taking into account non-local (gradient dependent) part of energy estimated by Eq.6.7. Corresponding refinement reads

$$e_{loc} = H_0(1 - S_y) + \pi Dk_0 S_x^2 + \pi(2 - Dk_0)S_z^2 \propto 1 - S_y + H_m S_z^2 / 2H_0 \approx (S_x^2 + p^2 S_z^2) / 2, \quad (4)$$

$$\frac{H_m}{H_0} \equiv \frac{4\pi(1 - Dk_0)}{H_0 + 2\pi Dk_0}, \quad p = \left[1 + \frac{H_m}{H_0} \right]^{1/2}$$

where k_0 is module of dominating wave-vector (for loop inductors, $|k_0| \approx \pi/l$) and the condition $Dk_0 \ll 1$ is taken in mind. For comparatively short-wave chaos, this is better invariant of fast motion (precession) than what defined by (6.6).

7.8. PHASE SLIPS AND NOISE PRODUCTION.

Plots (D) and (E) in Fig.18 show that when local amplitude of precession is passing through zero its phase can slip by some angle. In contrast to ideal black solitons (see Sec.5.6), this angle can take any value different from $\pm\pi$. Of course, usually two close spins undergo the same slip, but sometimes one or another spin can be beaten from common behavior. Hardly this fine detail of magnetization dynamics is unambiguously determined by a few relevant chaotic variables. Therefore, local phase slips may become the source of some amount of noise, in addition to chaos.

Although, by our observations, this noise is rather weak, probably it may create obstacles to ideal copying of chaos under synchronization.

7.9. QUASI-PERIODIC CHAOS.

Fig.19 illustrates example of quasi-periodic chaos obtained in auto-generator with relatively narrow loop antennae ($l = 0.2$ mm) at moderate gain ($=9$) and output saturation ($I_{sat} = 55$ mA), and antennae separation $x = 4l$. Dominating wave-length of magnetization pattern is close to $\lambda = 2l$ while carrier frequency of its oscillations is rather close to frequency of DE wave with $k_x = 2\pi/\lambda$ and $k_y = 0$.

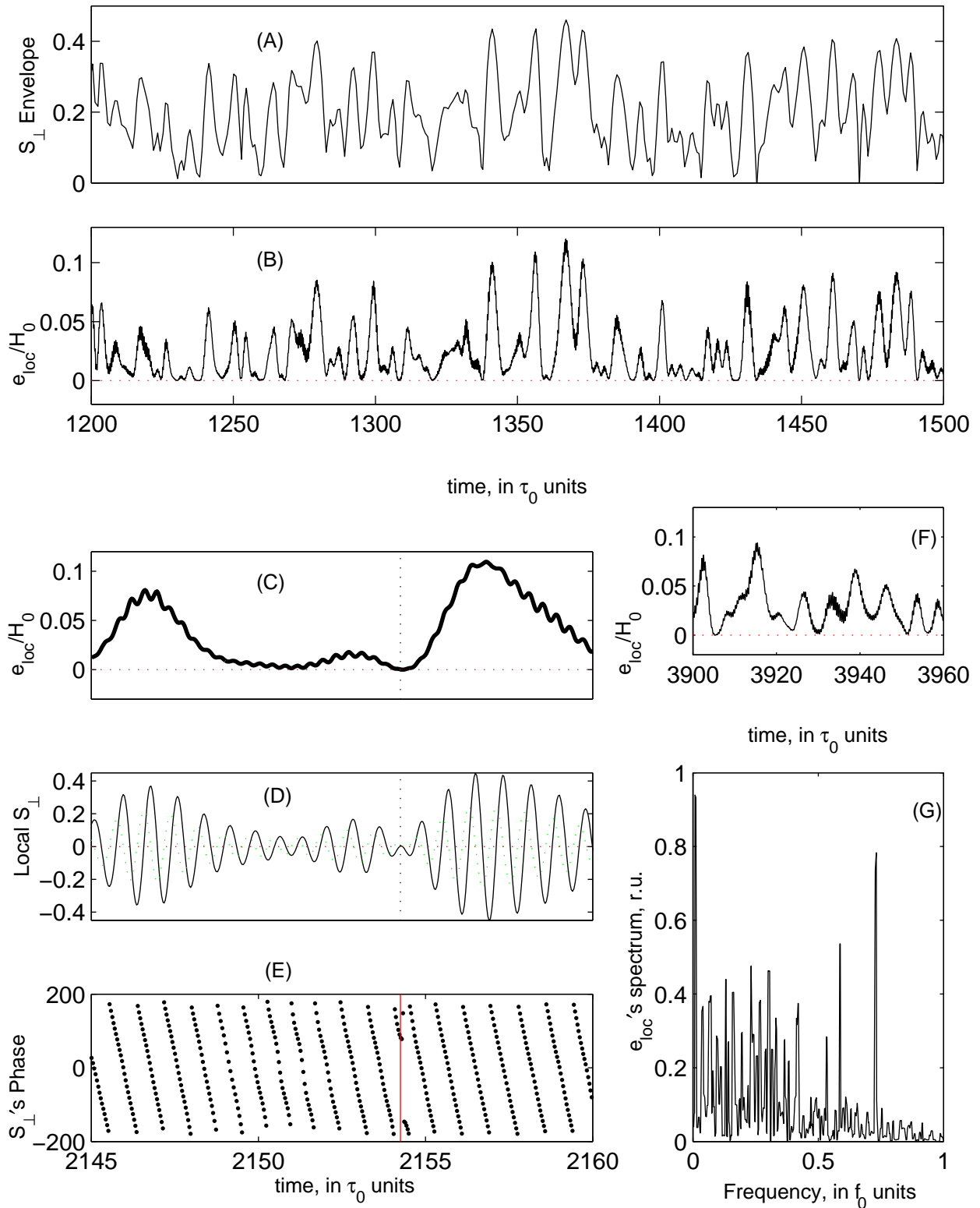


Fig.18. Instantonic temporal structuring of chaotic magnetization pattern and noise production. (A) Envelope of local $S_{\perp x}$ at particular point in vicinity of passive inductor. (B) $e_{loc}/H_0 \propto |\Psi|^2$ where e_{loc} is quasi-local energy density in the same particular point. It is almost free from high frequencies thus behaving as integral of fast motion. But in slower time scale it regularly turns into exact zero, demonstrating solitonic self-organization of magnetic energy. (C) Zero of $S_{\perp x}(r_0, t)$. (D) Simultaneous $S_{\perp z}$ (dot line) and $S_{\perp x}$ (solid line). (E) The zero results in random phase slip of spin precession, thus generating phase noise. (F) More zeros. (G) e_{loc} 's spectrum.

In this case, time series of different variables (magnetic energy, magnetization and voltage envelopes and phases, instant frequency, etc.) possess characteristic features of the kind of chaotic attractor termed noisy limit circle. The voltage spectrum at plot (F) resembles ruled spectra of complex periodic signals (with period being inverse distance between neighboring spectral lines). Nevertheless, in fact voltage signal is chaotic and its fractal dimension, $d_{cor} \approx 3.25$ (see plot(G)) even indicates hyperchaos.

Plot (D) shows that in spite of large magnitude of instant frequency oscillations (~ 500 MHz) and therefore very wide total frequency band of generated signal (≈ 0.9 GHz) its phase modulation lies between well certain boundaries not exceeding $\approx 100^\circ$. From comparison of plots (D) and (E) it is seen that positive (negative) slope of time-smoothed phase trajectory corresponds to smaller (greater) energy, in accordance with negative non-isochronity of MW.

What here happens? The frequency separation of the three main groups of lines in plot (F), ≈ 270 MHz, is by its sense the frequency of soliton births near active inductor. Hence, one envelope soliton is born approximately each 3.7 ns. The group velocity of DE waves at operational frequency (see Eq.5.14) is $v_g \approx 10^7$ cm/s, therefore time of soliton flight from active to passive loop is about 8 ns. Mean duration of one cycle of the quasi-periodic modulation can be estimated from plot (E) as ≈ 40 ns. Comparing these numbers we conclude that two solitons simultaneously are in action and that each cycle contains birth and transfer of $10 \div 12$ solitons. What is for the cycle duration itself, seemingly it can be connected to the relaxation time, Γ^{-1} .

7.10. ROLE OF FILM WIDTH TO WAVE LENGTH RATIO.

Intuitively, one may predict that formation and propagation of envelope solitons is sensitive to the ratio w/λ where w is width of film and λ ($\lambda \approx 2l$ for two-element loop antennae) is dominating wave length in magnetization pattern. The Fig.20a shows that, indeed, this is confirmed by numerical simulation of auto-generation in narrow (in the sense that $w \lesssim \lambda$) and wide ($w > \lambda$) films.

In narrow film, soliton takes all width of a film. In wide film, at very beginning of next soliton manufacturing one energy clot may be inflated occupying all the width but soon it breaks into two or three (or even more) solitons each of which takes a part of the width only. Then solitons run not in parallel to film boundaries but along one of two easy propagation directions which correspond to maximum group velocity (see Sec.5). Fig.20a demonstrates

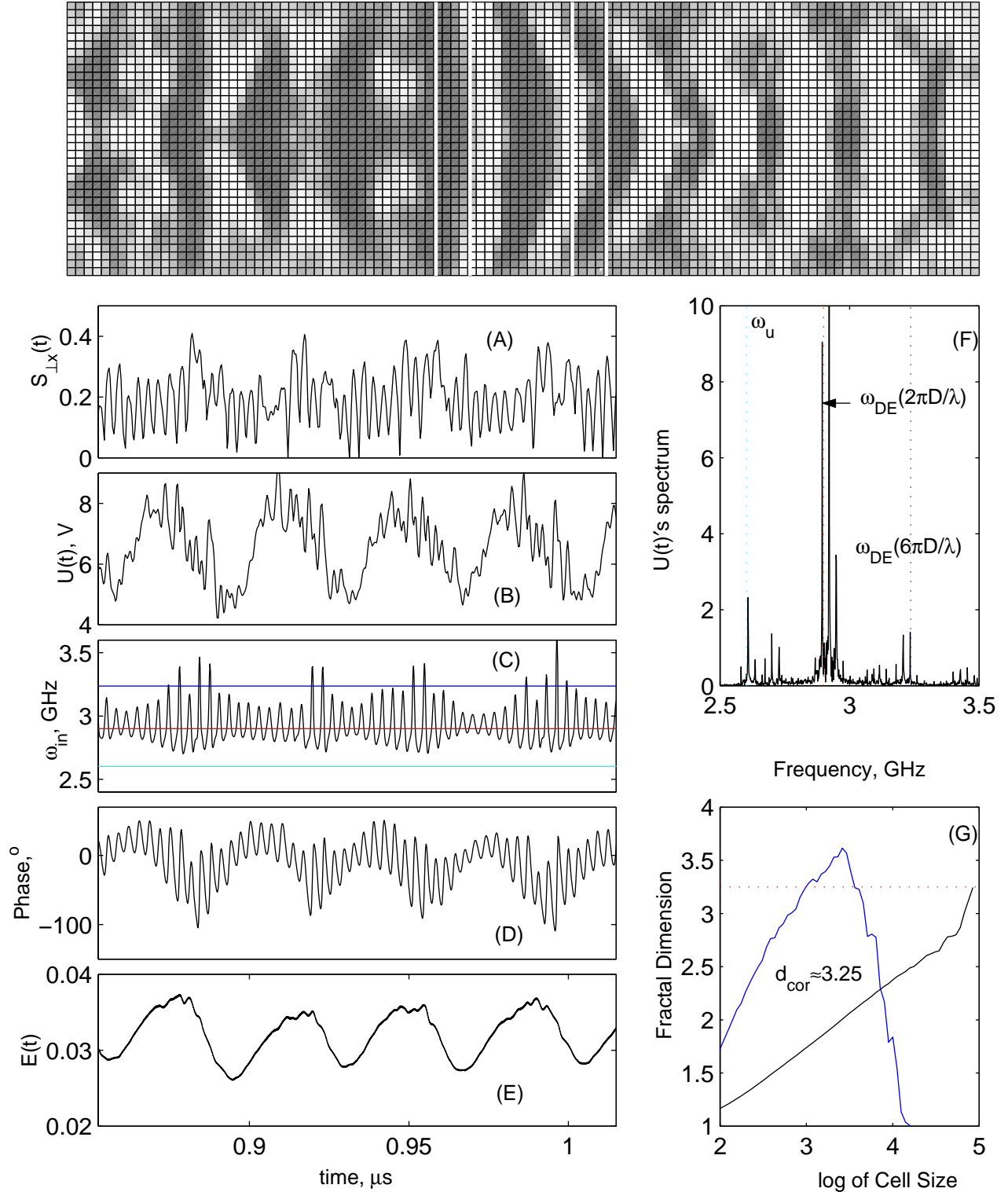


Fig.19. Noisy limit circle in auto-generator with the parameters: $H_0=400$ Oe, $\gamma=0.001$, $R_0=50$ Ohm, $C_0=0.5$ pF, $L_0=5$ nH, $U_{sat}=1$ V, $I_{sat}=55$ mA, Gain=9, $D=10\mu$, loop width $l=0.02$ cm, loop separation $x=0.08$ cm. The primarily excited DE MSW mode has wave length $\lambda=2l$. (Top) Instant $S_{\perp x}$ pattern. White lines show positions of two loops. (A) Envelope of local $S_{\perp x}$ in vicinity of left (active) loop. (B) Envelope of voltage, $U(t)$. (C) $U(t)$'s instant frequency and (D) corresponding phase oscillations. (E) Excess energy. (F) Voltage spectrum is typical one for quasi-periodic signals. (F) $d_{cor} \approx 3.25$.

Horizontal lines in (C) and dotted lines in (F) mark ω_u , $\omega_{DE}(2\pi D/\lambda)$ and $\omega_{DE}(3\cdot 2\pi D/\lambda)$. The MSW group velocity $v_{gr} \approx 10^7$ cm/s. Time of soliton flight between loops is $x/v_{gr} \approx 7.5$ ns. The circle period, ≈ 0.04 μ s (see (E)), is close to relaxation time, $\Gamma^{-1} \approx 100\tau_0$, and contains ≈ 11 solitons.

this for the case when two soliton chains are created (of course, if three or five soliton chains realize then central of them moves in parallel to boundaries).

Importantly, in general in wide film (at $w/\lambda \gtrsim 3$) wave fronts (equal-phase lines) of magnetization pattern stronger are curved then in narrow film (especially in region where different soliton chains meet one another). Therefore, the wider is film the smaller is voltage (EMF) per unit length induced in direct antenna, up to that wider film can produce lower voltage (at the same precession angle) which worsens the feedback.

As example of unpretentious situation, Fig.21 presents movie of one cycle of chaotic soliton generation in moderately pumped narrow film.

7.11. ABOUT COHERENCE OF AUTO-GENERATION.

It is known that spectrum of any oscillation with arbitrary amplitude modulation and arbitrary (let random) but limited phase modulation consists of infinitely narrow line (at carrier frequency) surrounded by some pedestal. An unlimited phase modulation that is accumulation of phase slips only produces a broadening of the carrier line.

In our numerical simulations of the auto-generation (even concerning strongly chaotic regimes) accumulation of phase slips (phase diffusion) on the average did not exceed one-two periods of carrier frequency per microsecond. Hence, coherent generation was observed, to the extent of calculation duration (apparent broadening of carrier line on spectrum plots is artifact of short-time Fourier transform).

Theoretically, the degree of coherence of chaotic generation is interesting open question. From practical point of view, it may be better answered in real experiments which reflect realities (like temperature instability) not accounted for by numerical model.

7.12. SPATIAL DIFFERENTIATION OF AUTO-GENERATION SPECTRUM.

Under auto-generation, magnetization in the whole film oscillates coherently. Due to chaotic soliton production, local phases of common oscillation undergo chaotic deviations which however remain limited (usually not greater then $\pm 60^\circ$). Local phase slips do not destroy common coherent picture.

But, of course, details of pedestal of oscillation spectrum may strongly depend on what variable is under measuring. This statement is illustrated by Fig.20a.

The Fig.20a corresponds to wide film, with $w/\lambda = 5$ and comparatively large separation of loop inductors, $x = 3\lambda$. It presents example of rather wideband chaos with complicated spectrum which in 6 peaks can be resolved. Again, the distance between central (most

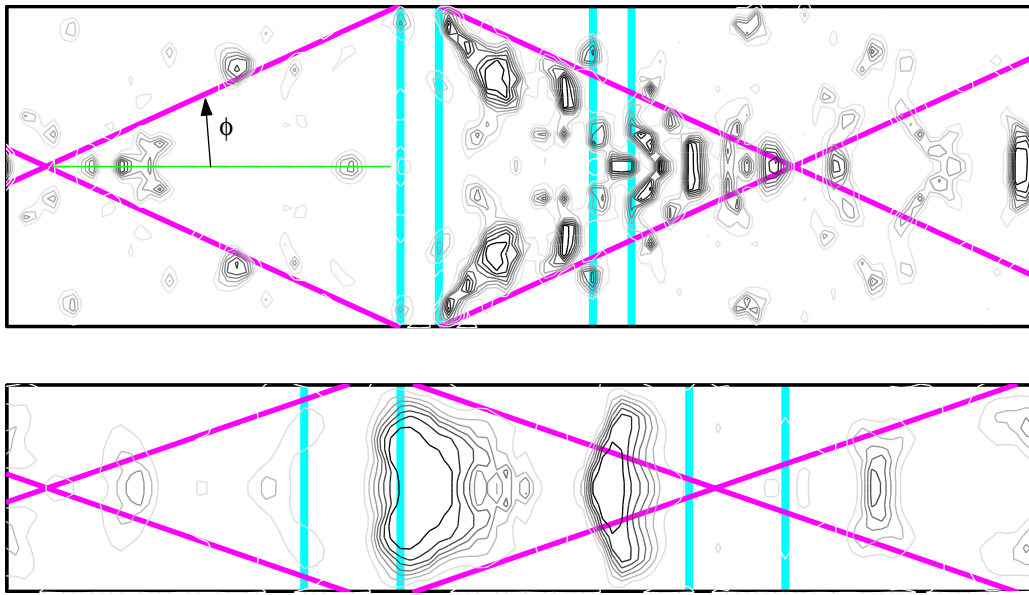


Fig.20a. Difference of soliton patterns in wide film (with width, w , greater than S_{\perp} 's wavelength, λ) and narrow film ($w < \lambda$). Vertical lines show inductors. The inclined lines show directions of most easy (fast) soliton propagation ($\tan \phi = (H_0/4\pi M_s)^{1/2}$). (Top) Energy density, e_{loc} , under chaotic auto-generation in wide film. Two soliton chains flow from active loop along easy directions. (Bottom) In narrow film, one soliton per its width can be placed only.

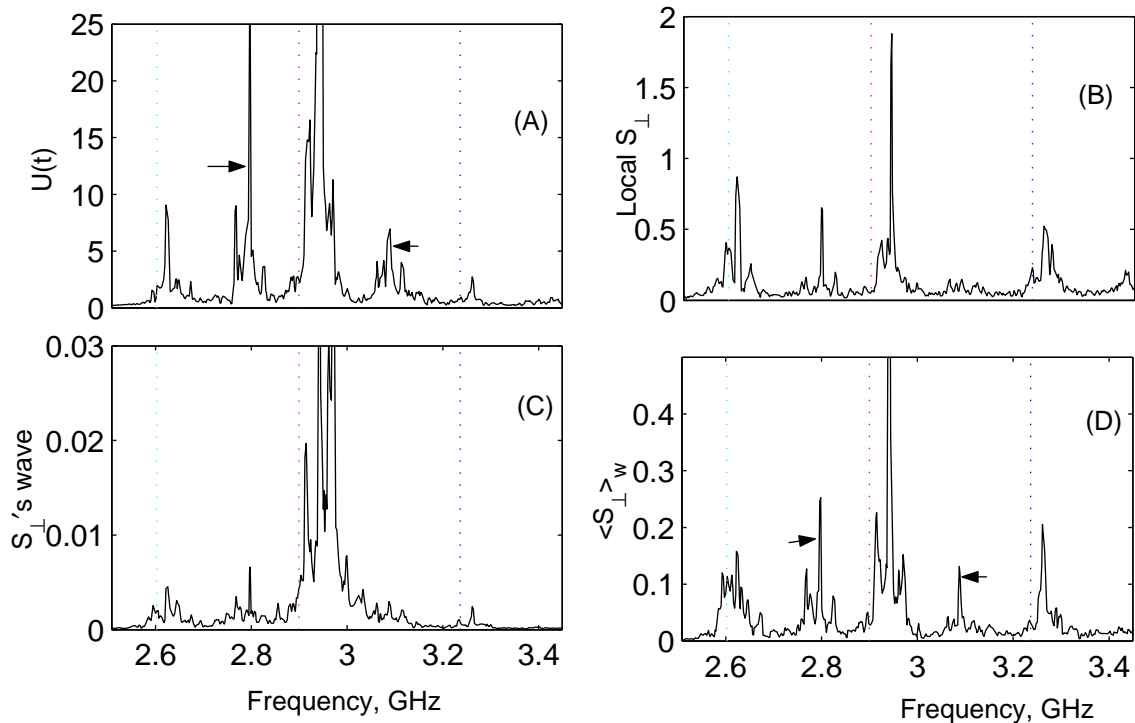


Fig.20b. Different variables have different spectra under the same chaos. (A) Voltage spectrum in wide film at $w=0.2$ cm, $\lambda=2l=0.04$ cm, $x=3\lambda$, $H_0=400$ Oe. (B) Spectrum of local spin precession, S_{\perp} , about center of film. (C) Spectrum of the expected induced plane-wave, $\int \exp(-2\pi i x/\lambda) S_{\perp} dr/V$. (D) Spectrum of width-averaged magnetization, $\int S_{\perp}(x,y) dy/w$, at x taken about right-hand edge. Dotted lines mark ω_u , $\omega_{DE}(2\pi D/\lambda)$ and $\omega_{DE}(3 \cdot 2\pi D/\lambda)$. The distance between highest peak and two peaks marked by \rightarrow and \leftarrow in (A) and (D) equals to inverse time separation of solitons, $\approx 1/(7$ ns). Naturally, spectrum (B) is most broad (up to 1 GHz) and most representing ω_u .

powerful) carrier peak and its closest neighbors equals to inverse mean time separation of soliton births. Approximately twice larger distance between the carrier and next two neighbors can be interpreted as second harmonics of the births frequency. Naturally, the carrier peak is most brightly represented in spectrum of spatial Fourier transform of magnetization at $k = \{2\pi/\lambda, 0\}$ (plot (C)) and least brightly in spectrum of local spin precession (plot (B)).

7.13. CIRCUMFERENTIAL SYNCHRONIZATION OF AUTO-GENERATION.

Naturally, the question arises about possibility of synchronization of chaotic auto-oscillations in one generator by voltage signal taken from another (at least identical) generator. Firstly, we tried to use voltage (EMF), $u_M(t)$, of additional wire inductor placed at right-hand end of the master film (i.e. behind the feedback inductor). This voltage was compared with voltage, $u_S(t)$, produced in identical control inductor in the slave film. The difference, $u_S - u_M$, was transformed into current, $J_{syn}(t)$, passed through one more wire inductor close to the control one, as shown in Fig.22. Notice that in case of exact coincidence, $u_S - u_M = 0$, the synchronizing current turns into zero, $J_{syn} = 0$, and thus slave film feels no difference from master film.

Paradoxically, because of almost ideal coherence of chaotic auto-generation, at available duration of numerical experiments, high-frequency (carrier) synchronization is automatically executed and thus calls no problem. The problem consists of synchronization of phase and amplitude chaotic modulation.

Films with $w/\lambda = 3$ were investigated. Various linear and non-linear (saturated) connections between $u_S - u_M$ and J_{syn} were tested, but none of variants has shown an evident superiority. Typical results are illustrated by plots (3)-(8) in Fig.22 which show three pieces of synchronization with respect to envelopes of feedback voltages in the master and slave, $U_M(t)$ and $U_S(t)$ (see scheme in Fig.15), and to their instant frequencies.

Undoubted signs of partial synchronization can be noticed already in 100 ns after beginning of the process. They become better visible if take into account obvious delay of the slave response. Plots (9) and (10) show how the picture looks if correction by delay is made. Most of details of signal $U_M(t)$ circulating in feedback device of master generator are reproduced by similar signal $U_S(t)$ in the slave. According to plot (2), high-frequency (carrier) phase difference between these signals does not leave the frame $\pm 80^\circ$. Nevertheless, in respect to the modulation there are essential quantitative and sometimes qualitative

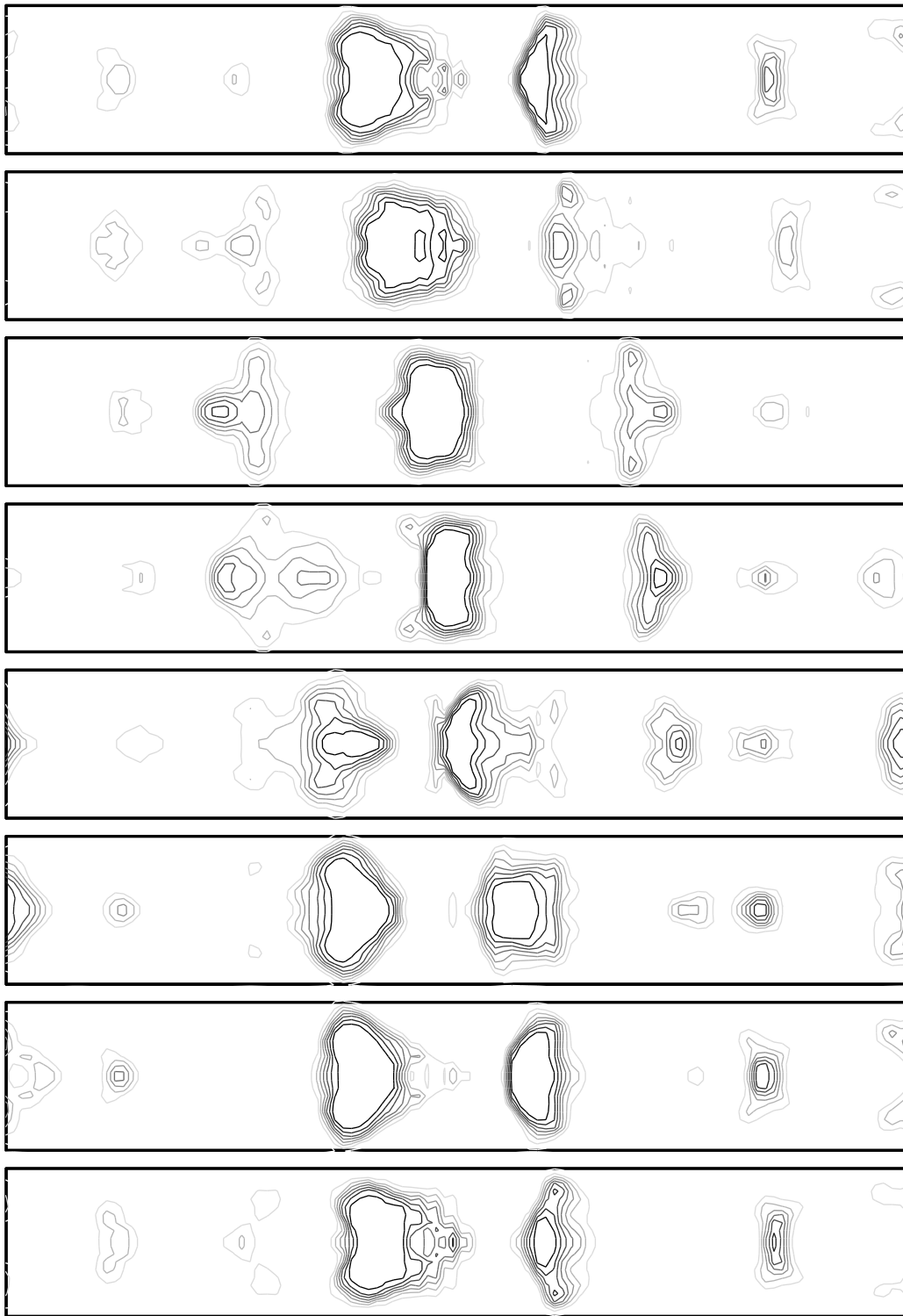


Fig.21. One cycle of quasi-periodic MSW envelope solitons auto-generation in narrow film ($w < \lambda$), at $H_0 = 500$ Oe, $\lambda = 2l = 0.1$ cm, $x = 2\lambda$, $\gamma = 0.0007$, $I_{\text{sat}} = 35$ mA, $U_{\text{sat}} = 1$ V, Gain = 6.7.

The circle duration ≈ 10 ns. The contour plots show instant spatial distributions of quasi-local energy density, $e_{\text{loc}}(x, y, t) = 1 - S_{\parallel} + H_m S_{\perp}^2 / 2H_0$. It is seen that in the greatest part of time two solitons are present only.

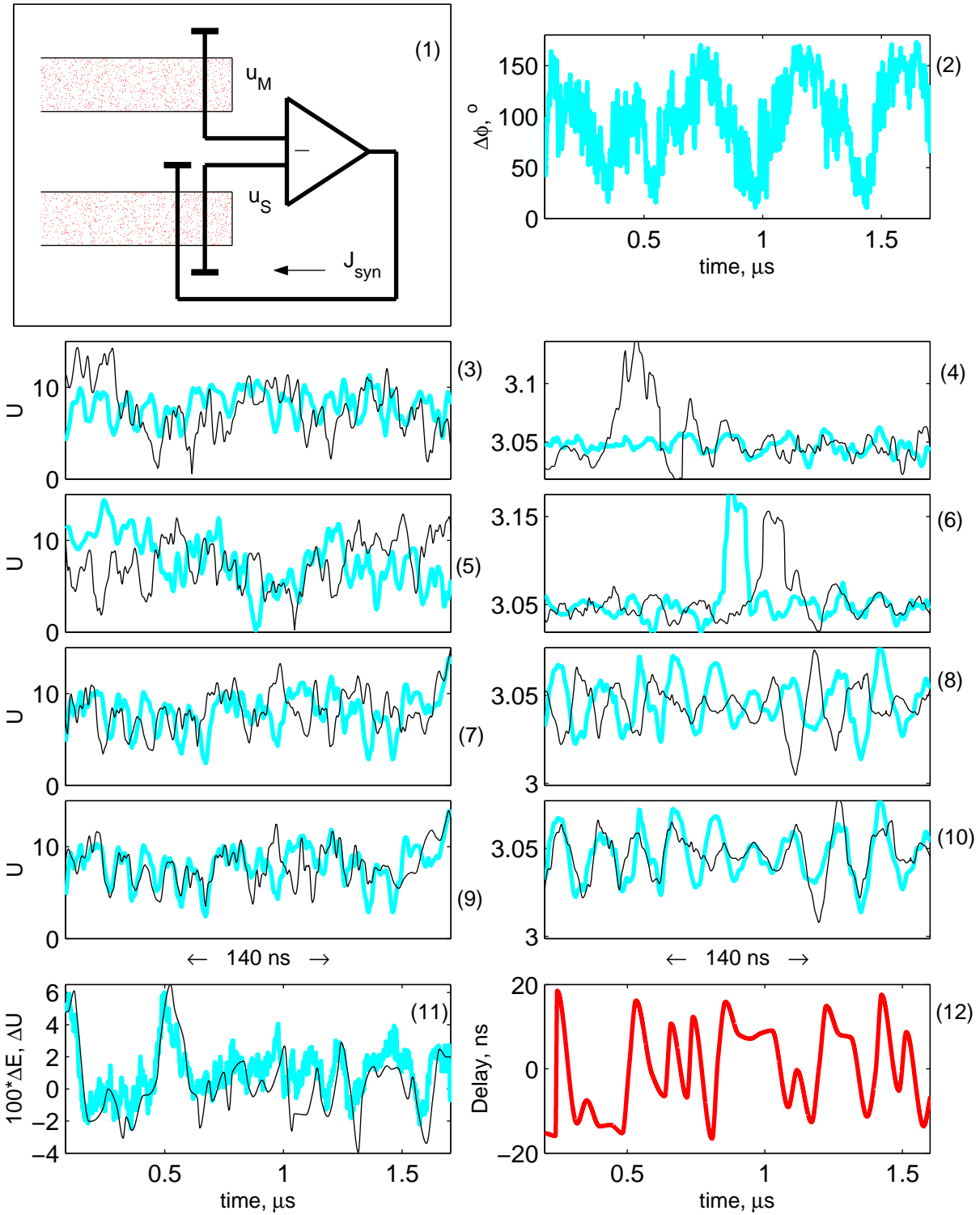


Fig.22. High-frequency chaos synchronization in Slave film by voltage signal taken from edge of another identical Master film. (1) Voltage difference between edge inductors, $u_S - u_M$, produces synchronizing current, J_{syn} , influencing the slave. (2) Phase difference between feedback voltages $U_S(t)$ and $U_M(t)$ (see Fig.15). (3) Amplitudes of feedback voltages (in V) and (4) their instant frequencies (in GHz) at start of synchronization. Fat (thin) curves relate to master (slave). (5)–(8) Same at two later time intervals. (9)–(10) Comparison of amplitudes and frequencies shown in (7) and (8) if accounting for delay of synchronization and energy background. (11) Correlation between difference of U_S and U_M amplitudes (thin curve) and difference of the slave and master energies (fat curve). (12) Delay via time.

distortions. The results are far from copying of chaos. To estimate them we need in a more soft criterion for partial synchronization.

7.14. DEFECTS OF SYNCHRONIZATION.

Careful analysis of data reflected in Fig.22 yields that most part of misalignment between $U_M(t)$ and $U_S(t)$ can be related to two reasons: (i) not constant but slowly time-varying delay, $\Delta T(t)$, and (ii) slowly time-varying amplitude shift which is in close correlation with difference between energies of master and slave film, $\Delta E(t) = E_S(t) - E_M(t)$. The latter statement is confirmed by plot (11). Notice that the delay, as shown at plot (12), may be both positive and negative (which corresponds to anticipating synchronization). This findings mean that, approximately, the relation

$$U_S(t) \approx \xi[E_S(t) - E_M(t)] + U_M(t - \Delta T(t)) \quad (5)$$

takes place with some coefficient ξ . Characteristic time scale of variations in $\Delta E(t)$, in amplitude shift $\xi\Delta E(t)$ and in the delay $\Delta T(t)$ too, are about ten times slower than variations in phase and amplitude of $U_{M,S}(t)$ during a cycle of soliton production.

Hence, the conclusion arises that some low-frequency component of the chaotic dynamics is not sensitive to synchronizing signal and therefore hinders to synchronize fast components which themselves are rather sensitive. Additional surprising evidence for this is that sharp switching from one master signal, $u_M(t)$, to another (may be the same but shifted by a time) temporarily improves synchronization which then becomes spoiled at longer time scale.

7.15. SYNCHRONIZATION BY FEEDBACK SIGNAL.

Seemingly, better synchronization will be achieved if synchronizing signal is taken from the “heart” of generator, i.e. from the feedback device. In the simplest variant shown by plot (A) in Fig.23, the master feedback voltage mix up with the slave one, with some coefficient α .

In this experiment besides the control voltages, $u_S(t)$ and $u_M(t)$, were under comparison taken from wire inductors placed between active and passive loops (see plot (B)). At $\alpha = 0.4$, best results of synchronization with respect to the power absorption, $P_{M,S}(t)$, amplitude of control voltage, $u_{M,S}(t)$, and amplitude and instant frequency of feedback voltage, $U_{M,S}(t)$, are presented by four center plots in Fig.23. Again, here slow time-varying delay between Slave and Master signals and slowly difference in their magnitudes

were found, in correspondence with Eq.5. Similar correlation between difference in power absorption and difference in film energies is detected in plot (C).

Plot (F) allows to see what the events develop in a concrete point marked by star at plot (B) (which itself represents a snapshot of quasi-local energy pattern). The new interesting observation follows from the histogram (probability distribution) of delay, at plot (E). Sharp peaks in this plots are separated by ≈ 0.35 ns which is close to period of precession. This may be hint on fine features of synchronization still to be understood.

Clearly, a kind of rough synchronization takes place, but in details it looks even worse than in the above circumferential case.

Therefore stronger mixing with $\alpha = 0.8$ was tested. Its results are shown in Figs.24a-b (see captures to these figures). According to top four plots in Fig.24a, results occurs definitely better than at $\alpha = 0.4$. This improvement is directly connected to essentially smaller difference between carrier phases of $U_S(t)$ and $U_M(t)$ (plot (4) in Fig.24b) than in previous case (plot (D) in Fig.23).

7.16. MORE ABOUT DEFECTS OF SYNCHRONIZATION.

From the power and feedback voltage time series it is seen that most of maxima and minima corresponding to soliton births are well reproduced by slave system. However, synchronization of events in the interspace between driving and feedback inductors is rather bad as registered by the powers, $P_{M,S}(t)$, and control voltages, $u_{M,S}(t)$, in Fig.24a. This means that magnetization pattern in slave film imitates that in master film but never copies it.

This misalignment can be explained as follows. There is no rigid connection between film energy and a number of solitons. Some background (smoothly distributed and slowly varying) part of energy behaves more or less autonomously and remains out of synchronization. Plots (1)-(5) in Fig.24b demonstrate that all the characteristics of instant (time-local) quality of synchronization are closely correlated with difference between the energy backgrounds in slave and master films. Plot (C) shows that (in concrete case under consideration) characteristic frequency of chaotic variations of energy background is about 30 MHz, which is of order of inverse relaxation time, Γ^{-1} .

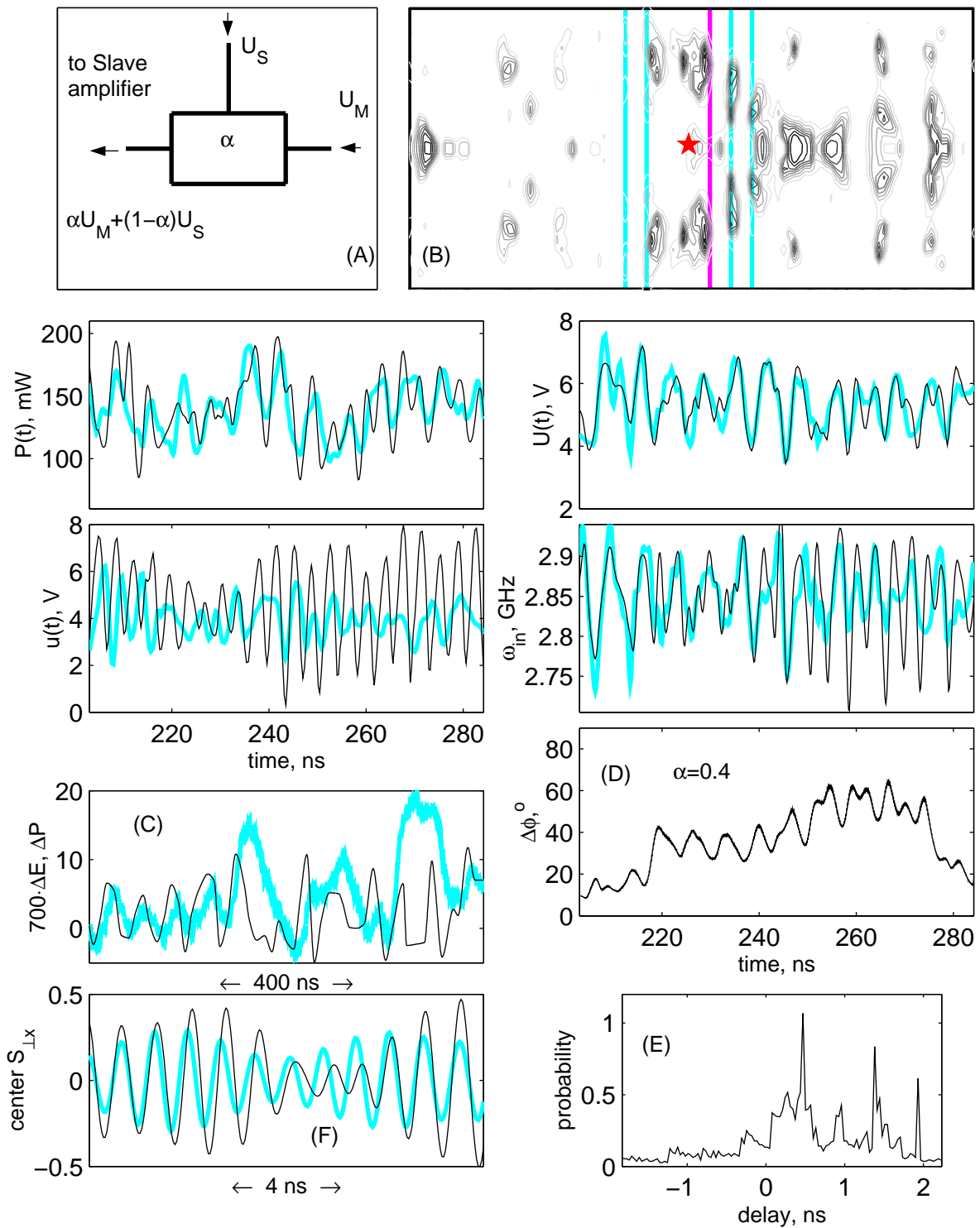


Fig.23. Synchronization of chaos in Slave generator by mixing its feedback (passive loop) voltage, $U_S(t)$, with feedback voltage from Master film, $U_M(t)$. (A) Mixing with the coefficient α . (B) Wide film under investigation. Two left and two right lines show active and feedback loops and central line additional control inductor. The four plots below demonstrate best results if $\alpha=0.4$. The powers, P , feedback voltage amplitudes, U , its frequencies, ω_{in} , and envelopes of voltage on the control inductor, $u(t)$, in Master (fat curves) and Slave (thin curves) films are compared with corrections to time-dependent delay and energies. (C) Correlation of power's difference and energies difference. (D) High-frequency phase difference between U_S and U_M . (E) Watching for phase coherence of spin precession at points marked by the star in (B). (F) The time delay histogram shows that delay is nearly quantized by period of precession, ≈ 0.35 ns.

Fig.24c presents one more example of the same kind of synchronization, with $\alpha = 0.9$, at wide film ($w/\lambda = 5$) in strongly chaotic regime. Under corrections to influence by non-synchronized energy background, the picture of synchronization with respect to power absorption looks enough good (plot (D)). But the whole picture has no significant differences from previous case.

7.17. MAGNETIC TURBULENCE.

The Figs.25a-b illustrate what happens at too powerful auto-generation which is achieved under weak output saturation, $I_{sat} = 100$ mA, although at relatively small linear gain ($=4$). In spite of that film is narrow ($w/\lambda = 2.5$), extremely chaotic shapeless energy pattern is formed by irregularly scattered solitons (see top picture in Fig.25b).

In this case (which may be named turbulent magnetic chaos), noticeable chaotic drift (diffusion) of the carrier phase takes place due to phase slips, as shown at plot (A) in Fig.25a. Plots (F)-(H) and (C)-(E) present well expressed slips in local magnetization and in such the integral characteristics as feedback voltage. According to plot (B), corresponding slow chaotic variations of carrier frequency are excellently anti-correlated with the energy (as the non-isochronity implies).

Two interest things should be appointed.

(i) In contrast to commonly strong chaos, with $d_{cor} \approx 3.9$ if estimated from feedback voltage time series (see plot (C) in Fig.25b), the energy behaves much more regularly and can be characterized by own fractal dimension, $d_{cor} \approx 2.7$. Possibly, this is just manifestation of above mentioned autonomy of the energy background.

(ii) Very slow chaotic variations in energy (and thus in the carrier frequency and other related values) are observed, with characteristic frequencies down to 3 MHz (plots (D) and (E) in Fig.25b).

7.18. CHAOTIC PULSE AUTO-GENERATION.

Slight decrease in linear gain (from 4 to 3) at the same film at same output saturation results in new interesting regime of auto-generation which is characterized by sharp pulses of the power absorption, $P(t)$, and voltages in feedback and driving loops, $U(t)$ and $V(t)$.

This example is illustrated by Figs.26a-b. Theoretically, $P = \langle JV - IU \rangle_T$, where $I(t)$ and $J(t)$ are currents in feedback and driving loops (see scheme in Fig.15), and $\langle \dots \rangle_T$ means averaging over period of precession. The part $\langle JV \rangle_T$ is power absorption

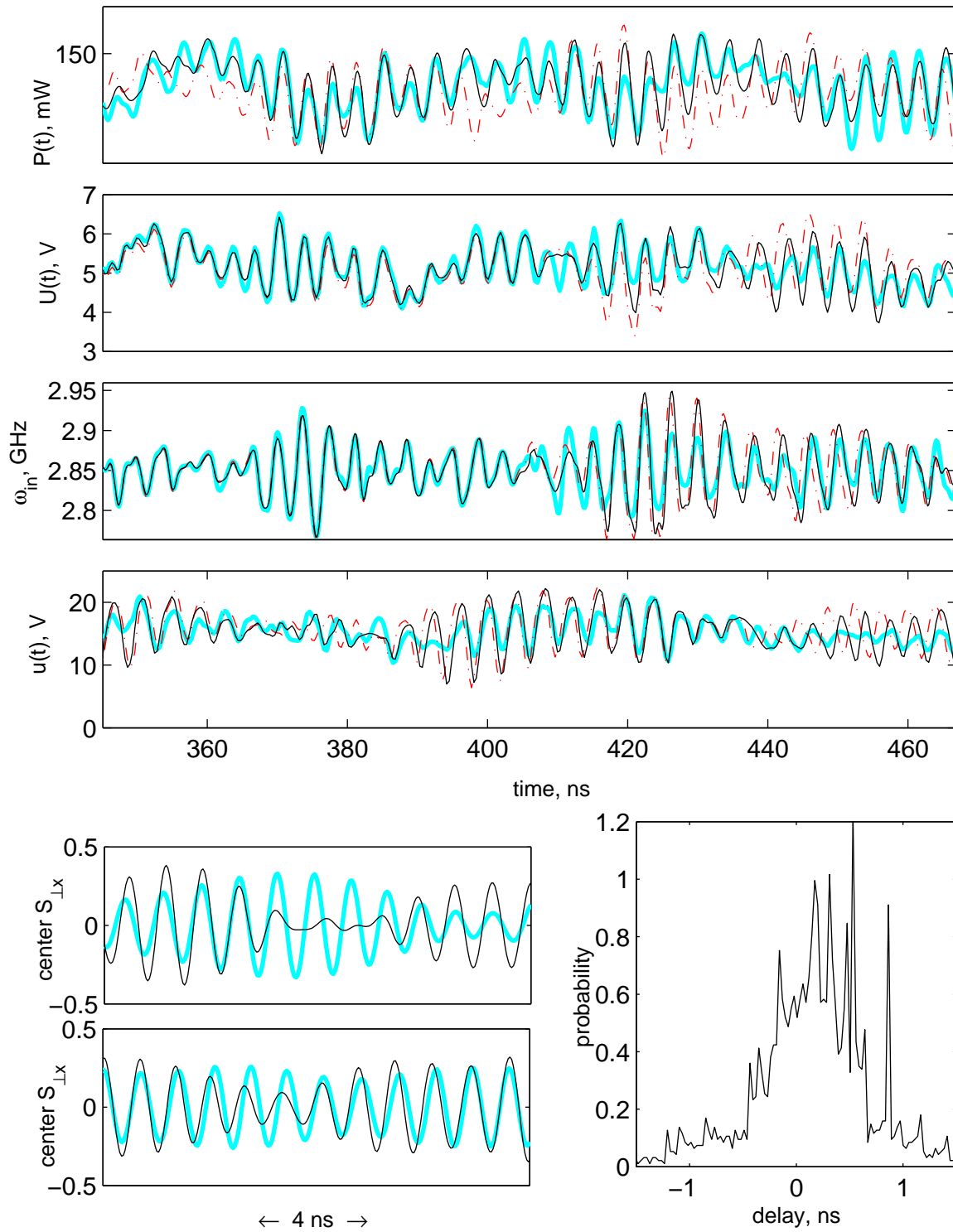


Fig.24a. Synchronization of strong chaos in wide film by mixing feedback voltages (see Fig.23,A) at $\alpha=0.8$. Other parameters: $H_0=400$ Oe, $\lambda=2l=0.04$ cm, $x=2.5\lambda$, $\gamma=0.0007$.

Typical time series of power absorption, $P(t)$, feedback voltage envelope, $U(t)$, its instant frequency, $\omega_{in}(t)$, envelope of voltage on the control wire inductor (see Fig.23,B), $u(t)$, and magnetization at film center, $S_{\perp x}$, are shown. Fat curves relate to Master. Dotted thin curves are actual Slave series. Solid thin curves are the latters but corrected by subtracting (i) time-variable delay of synchronization and (ii) difference of slowly varying energy backgrounds. The right-hand bottom plot is histogram (probability distribution) of the delay.

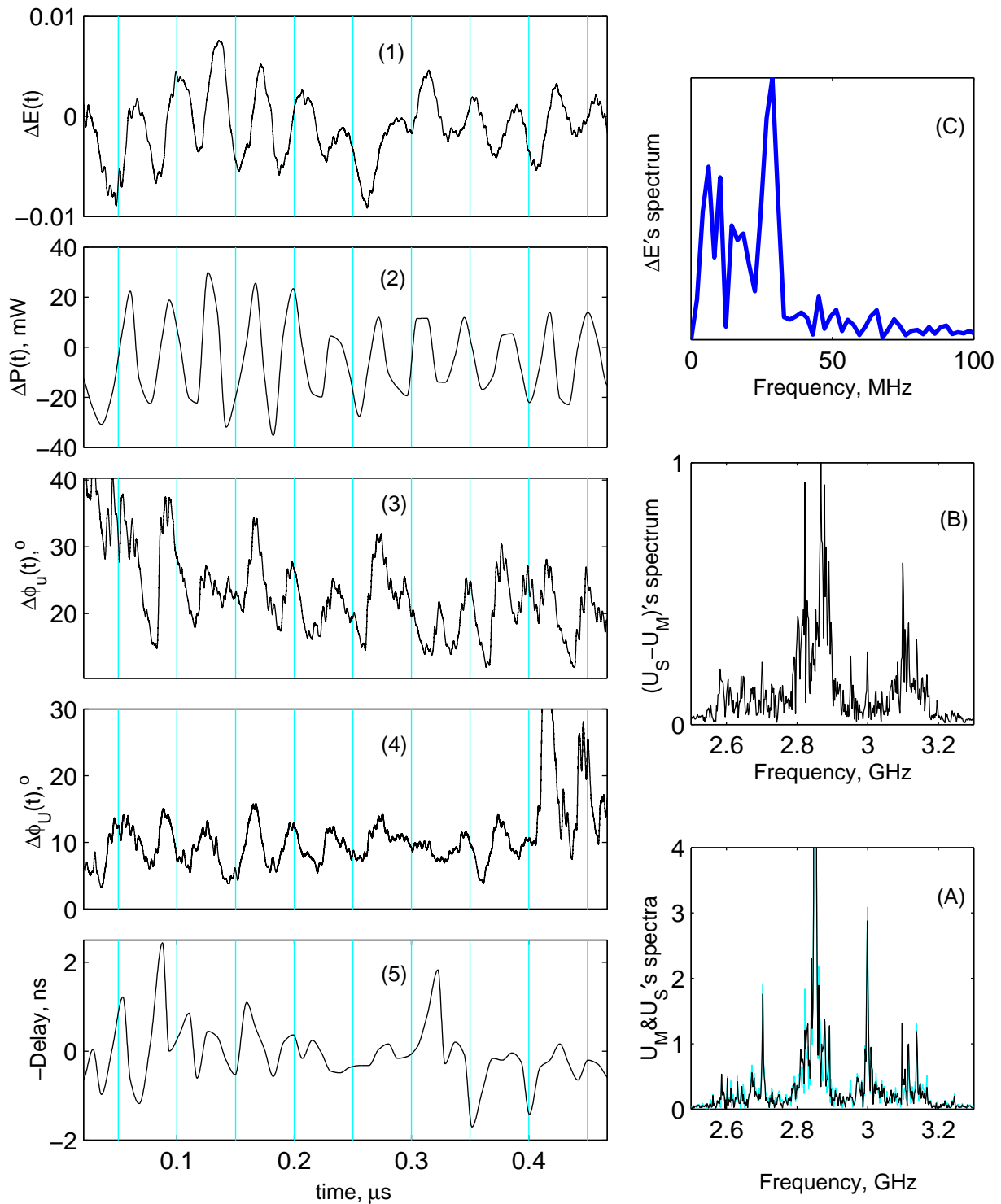


Fig.24b. Continuation from Fig.24a. Synchronization of strong chaos (see Fig.23,A) at $\alpha=0.8$. (1) Energy difference between Slave and Master films, $\Delta E(t)$. (2) Slow (time-smoothed) component, $\Delta P(t)$, of their difference in power absorption. (3) Microwave-band phase difference, $\Delta\phi_U(t)$, between voltages $u_S(t)$ and $u_M(t)$ on the control inductors (see Fig.23). (4) The same, $\Delta\phi_U(t)$, for feedback voltages $U_S(t)$ and $U_M(t)$. (5) Time delay of synchronization with respect to fast variations in power absorption caused by soliton's births. Rather pronounced correlation between all these variables are evident. (A) Spectra of $U_S(t)$ and $U_M(t)$. (B) Spectrum of $U_S(t) - U_M(t - \delta t)$, where δt , $\delta t \approx 0.01$ ns, is time delay equivalent of $\Delta\phi_U(t)$'s mean value in (4). (C) Spectrum of $\Delta E(t)$. Its characteristic frequency, ≈ 30 MHz, coincides approximately with central peak bifurcation in (B) and with energy relaxation rate, $2\Gamma \approx 2\gamma(H_0/M_s + 2\pi)/\tau_0$.

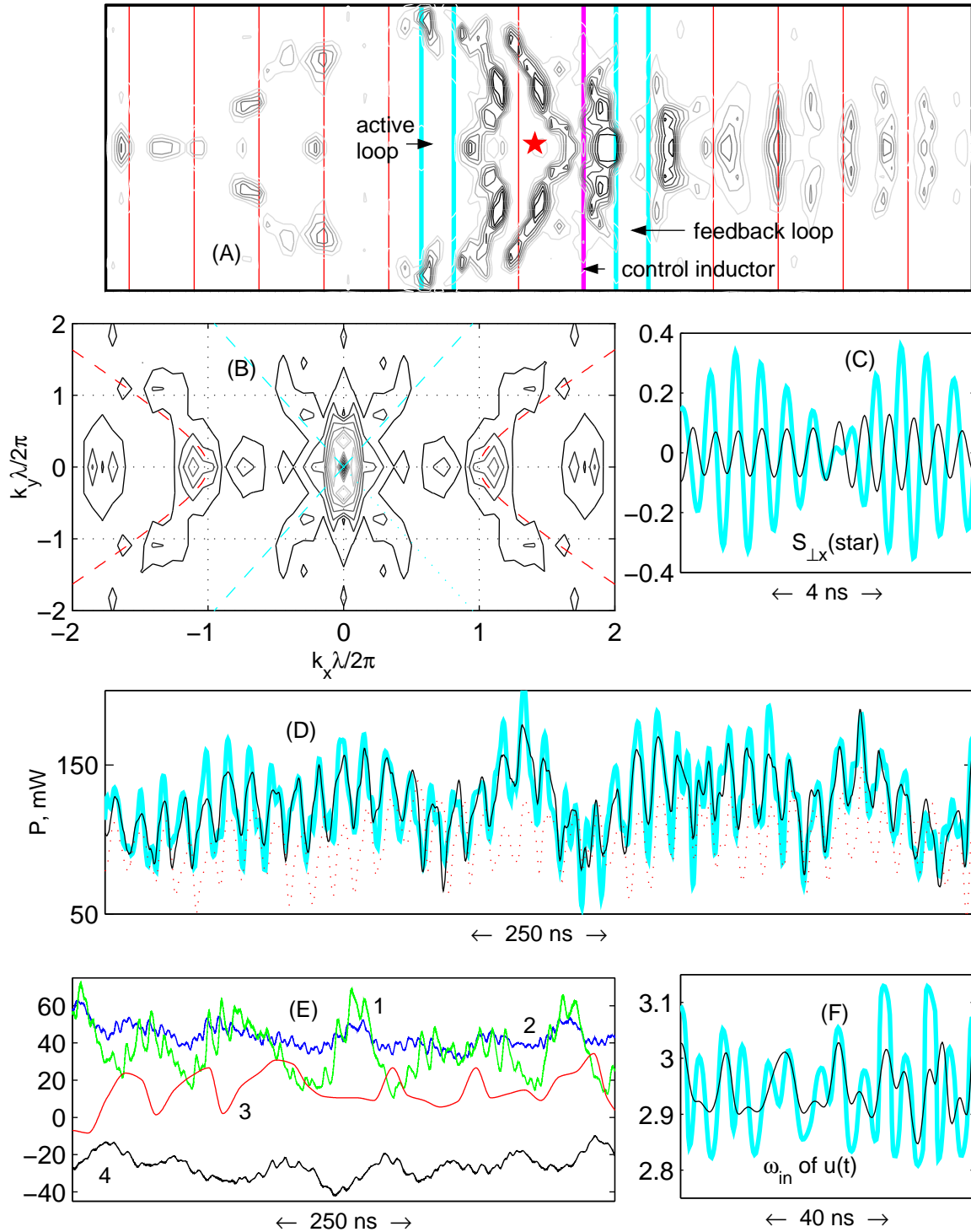


Fig.24c. Synchronizing hyperchaos (with $d_{cor} \approx 3.5$) in wide film ($w/\lambda=5$), at $\alpha=0.9$, $H_0=400$ Oe, $\lambda=2l=0.04$ cm, $x=3\lambda$. (A) Local energy pattern, $e_{loc}(x,y,t)$. The lines mark inductors (fat) and x -coordinates distanced by λ (thin). (B) Spatial Fourier transform of $e_{loc}(x,y)$. Clearly, separation of energy clots (solitons) equals to λ , while their width (in x -direction) is of order of $\lambda/2$. (C) Example of local phase slip in Master's precession (star at (A)) not imitated by Slave. (D) Power absorption by Master film (fat), by Slave film (dotted thin) and that shifted accounting for non-constant delay and slow energy fluctuations (solid thin). (E) $\Delta\phi_U$ (1), $\Delta\phi_U$ (2), delay in units of $\tau_0/7$ (3), and $2000 \cdot \Delta E$ (4). One can see mutual correlation of these time series. (F) Example of bad synchronization in respect to instant frequency of $u(t)$.

from driving loop which can be written as $\langle JV \rangle_T = |J||V| \cos(\phi_V - \phi_J)$, with $|J|$ and $|V|$ being envelopes and ϕ_V and ϕ_J phases. Fat curve and thin curve close to it at plot (5) in Fig.26b show pulsations of P and $\langle JV \rangle_T$, respectively, while the low-amplitude curve here represents $\langle IU \rangle_T$ and shows that the feedback loop is consuming film's energy.

In this case, again (i) essential difference between common chaos (with $d_{cor} \approx 3.3$) and particular energy chaos (with $d_{cor} \approx 2.2$), and (ii) slow energy variations (with characteristic frequencies ~ 2 MHz if not less) take place.

At last, due to relatively simple and expressively shaped chaos and relatively small fractal dimension in this case, we may try to draw three-dimensional projection of corresponding chaotic attractor. Two variants of the projection are shown in Fig.28.

7.19. ON POWER THRESHOLD OF CHAOS.

In numerical simulations, we can set any gain and output power as we want. In practice, small-sized high-frequency amplifiers have rather limited output power. Therefore, consider rough analytical estimate of the smallest (threshold) power absorption by film which is sufficient for chaotic auto-generation.

Time averaging of the energy conservation law (6.3), if combined with the relations (6.4) (at $E_0 = 0$ as it was seen) and (6.6) (i.e. for not too short-wave chaos), yields

$$\langle P \rangle_T \approx H_0 \Gamma \|S_x\|^2 \approx H_0 p \Gamma |\Psi|^2 = \omega_u \Gamma |\Psi|^2 , \quad (6)$$

where Ψ is the wave function considered in Sec.5, p is eccentricity of uniform precession, and $\langle P \rangle_T$ is mean power absorption per unit volume (in dimensionless units). Hence, in according with the estimates of the minimum $|\Psi|$'s value, A_{\min} , which initiates wave instability (see Sec.5.5), we can estimate power level (per unit volume) which is sufficient for beginning of chaos as

$$\min \langle P \rangle_T \approx \omega_u \Gamma^2 / |\varkappa| \quad (7)$$

In real units, for the total threshold power absorption, P_{thr} , in a film with volume V this formula implies

$$P_{thr} \approx 2\pi M_s^2 V f_u \Gamma^2 / |\varkappa| , \quad (8)$$

where f_u is uniform precession frequency (in s^{-1}) and Γ remains dimensionless.

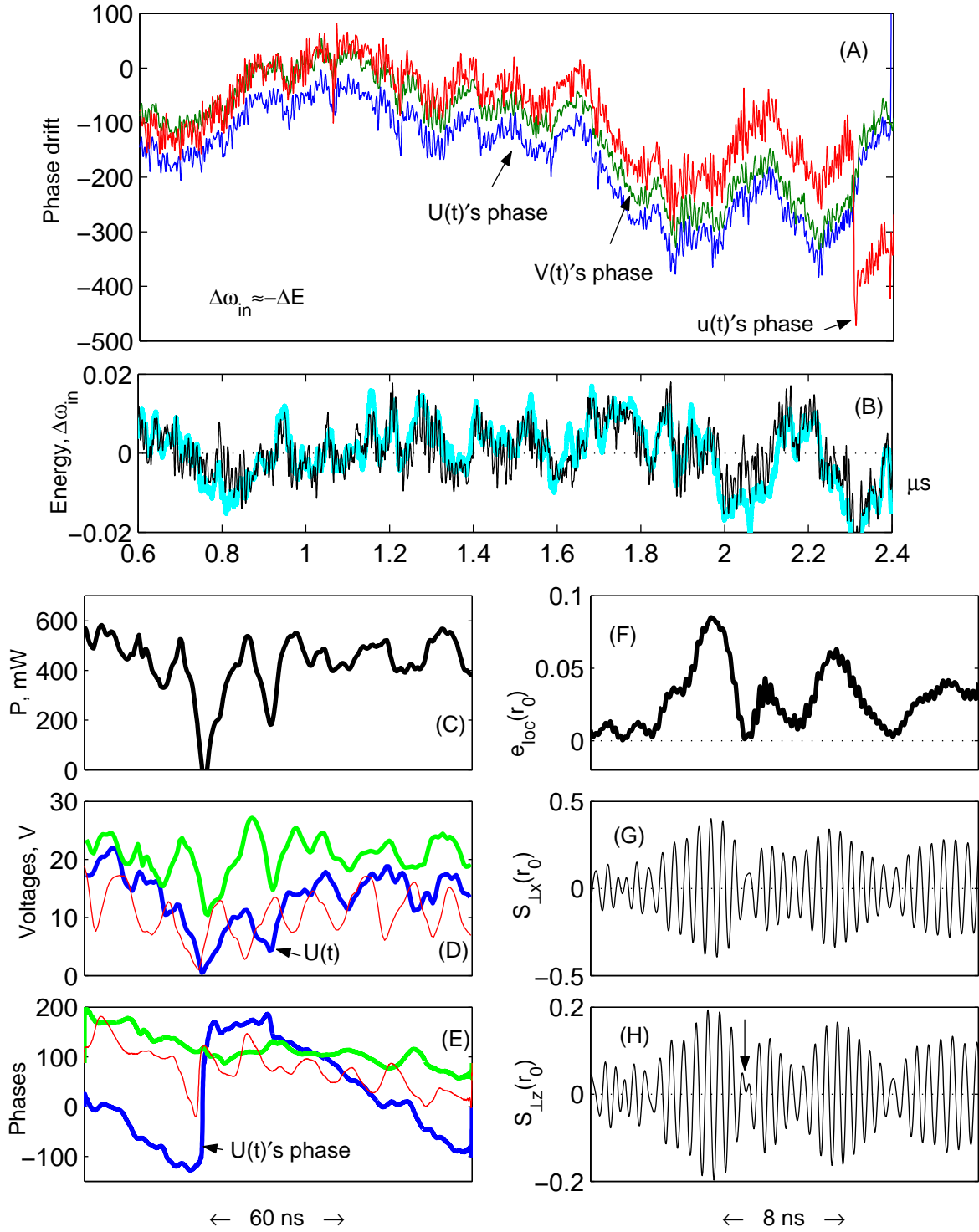


Fig.25a. Turbulence in strongly pumped film at $H_0=400$ Oe, $\lambda=2l=0.08$ cm, $x=2\lambda$, $w/\lambda=2$, $\gamma=7\cdot 10^{-4}$, $I_{\text{sat}}=100$ mA, $U_{\text{sat}}=1$ V, Gain=4. (A) Slow drift of phases of the feedback, control and active loop voltages. Slope of the drift is in close connection with slow energy variations. Both are characterized by frequency ≈ 20 and besides lower frequencies. (B) $E(t)-\langle E \rangle$ (fat light curve) as compared with time-smoothed instant frequency of $V(t)$ (thin dark curve). (C–E) Example of phase slip of feedback voltage. (F–H) Fragment of spin precession picture in the point $r_0=(x_0, y_0)$ marked by star in Fig.25b. The arrow shows the phase slip moment.

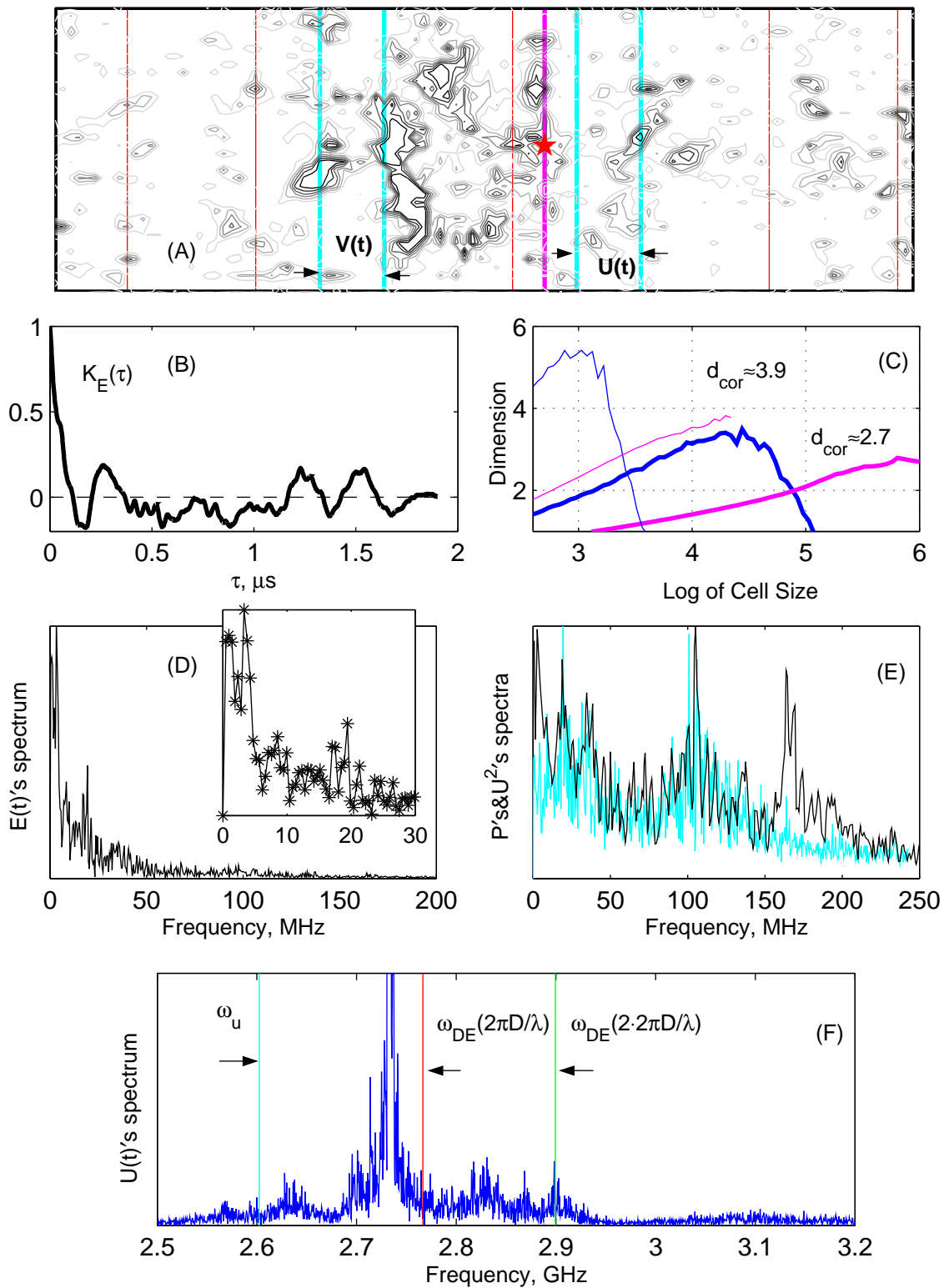


Fig.25b. Turbulence in strongly pumped film at $H_0=400$ Oe, $\lambda=2l=0.08$ cm, $x=2\lambda$, $w/\lambda=2.5$, $\gamma=7 \cdot 10^{-4}$, $I_{\text{sat}}=100$ mA, $U_{\text{sat}}=1$ V, Gain=4. (A) Distribution of energy clots is non-regular. (B) But energy correlation function, $K_E(\tau)$, discovers rather regular slow fluctuations in total film's excitation level. (C) Correspondingly, fractal dimension of energy signal (fat curves), $d_{\text{cor}} \approx 2.7$, is smaller than of $U(t)$'s envelope (thin curves), $d_{\text{cor}} \approx 3.9$. (D) The energy spectrum has characteristic frequencies ≈ 3 MHz (see inset) and ≈ 20 MHz. (E) The spectra of power absorption (dark curve) and of $U^2(t)$ (light curve) have also peaks at ≈ 100 MHz and ≈ 170 MHz related to mean period of soliton's births, ≈ 8 ns.

In YIG film, at $H_0 \approx 550$ Oe (i.e. ≈ 4 in dimensionless form) $|\alpha| \approx 1.4$ and $f_u \approx 3.2 \cdot 10^9$ s⁻¹. If take $\Gamma = 0.007$, which corresponds to approximately 1 Oe half-width of linear FMR, and the volume be 7 mm \times 2 mm \times 10 micron then Eq.8 gives $P_{thr} \approx 180$ mW. However, the estimate is rather sensitive to energy losses, and at 0.5 Oe half-width of FMR it turns into ≈ 40 mW. Probably, this is still overestimated value since not the whole volume must be critically excited at threshold pump.

Conclusion

We have reported selected results of work which was made in 2002-2003 years. Additional information about this work, - in the form of HTML presentation (also made at that time) with figures, movies and comments to them, - can be obtained by downloading and unzipping file http://yuk-137.narod.ru/experience/mfs_2002.zip. This presentation includes also some information about our (together with our colleagues) first attempts of practical generation and synchronization of magnetic-wave chaos and its properties in comparison with that observed in numerical simulations.

On the latter subjects and, besides, physical properties of our ferrite (YIG) films and first practical applications of electro-magnetic chaos, generated with the help of these films, to direct microwave-frequency secure communication, see also our recent journal articles [1,2].

Principal conclusions what can be extracted from the aforesaid material are as follow.

(i) There are two main mechanisms of the magnetic-wave chaos auto-generation. One is creation of non-regular chains of (“gray”) envelope solitons composed (in in-plane magnetized films under our above consideration) primarily with ‘surface’ (“Damon-Eshbach”) magnetostatic spin waves (MSW). Another mechanism is parametric energy transfer from these waves to relatively short “backward” MSW (“bulk” MSW) and reversed process.

(ii) The first mechanism dominates at not too large (in-plane) magnetizing field (therefore, generates lower carrier frequencies) but it needs in much smaller level of energy consumption (dissipation) in film and, hence, much smaller amplification in a feedback circuit. Besides, importantly, it produces much more “rich” chaos, which allows, in principle, to “hide” a large amount of information.

(iii) However, these advantages of the “parametric” chaos (as compared with the “soli-

tonic” one) are accompanied with probable instability of the parametric interaction between surface and backward MSW, which may take form of explosive and irreversible transfer of energy from surface to short backward waves. A degree of the irreversibility is as large as great is number of excited backward wave modes per one exciting surface mode. At some regimes of auto-generation one can observe from time to time fast and practically full energy swaps into short backward waves and, consequently, sharp and long-standing suppressions of auto-generation (sometimes, under definite conditions, it may break for periods up to nearly μs).

This phenomenon (in the presentation, we called it “parametric collapse”) was observed both in numerical and real experiments (with good correspondence between them, though numeric procedures inevitably loss most short waves). Naturally, it can create strong obstacles to synchronization of chaos, because the breaks of auto-generation imply uncontrollable and hardly reproducible in “slave” system) phase slips.

(iv) Therefore, to avoid the “parametric collapse” but, at the same time, exploit parametric processes as much as possible, it is necessary to introduce some auto-regulation of feedback amplification. It can help in generation of such output electromagnetic signals what possess not too strong amplitude modulation, at strong enough phase and frequency chaotic modulation, and cause satisfactory “synchronous chaotic response” in slave system.

(v) Fractal (correlation) dimensions of both high-frequency chaotic oscillations of different variables (local magnetization values, e.m.f.’s in antennae, and voltages and currents in feedback circuit) and low-frequency variables (amplitudes, phases and “instant frequencies”) almost always lie in interval from 2 to 4 and usually between 3 and 4, thus demonstrating “hyper-chaos”. This numeric result well agrees with fractal dimensions of low-frequency (amplitude and phase) signals obtained from real chaotic generators. At the same time, some of low-frequency variables, both real and numerical (e.g ‘quasi-local energy density’ and total “excess” magnetic energy) can show dimensions nearly by unit lesser, from interval $2 \div 3$.

(vi) These facts, seemingly, help to understand why, in spite of not high fractal dimension of the our chaos, we never observe “ideal synchronization”, instead seeing only what can be termed “generalized synchronization”. The matter is that, in the schemes under investigation, all the control and feedback signal are directly coupled with the “surface” (“Damon-Eshbach”) MSW modes only. This is obvious from comparison of voltage-current

spectra, - whose frequency band always lies near or higher the uniform precession frequency, - and numerically found spectra of local magnetization values (local precession) which can be concentrated mainly at twice lower frequencies or even four times lower ones (because of two successive parametric divisions of frequency), down to absolute lower bound of MSW spectrum (moreover, sometimes, - e.g. after the parametric collapse, - become concentrated just near this bound).

Therefore, it is not surprising if one of 4 effective relevant degrees of freedom of our system (the number 4 follows from fractal dimension between 3 and 4), - which is responsible for magnitude of short backward MSW and their energy exchange with surface MSW, - stays far out of control we used.

If this is true explanation of the generalized character of synchronization, then we have chances to improve the described results.

(vii) It appeared undoubt that even rather rough numeric simulations are useful not only for adequate theoretical of real experiments, but also for their planning.

Clearly, the described work leaved many unanswered questions and hypotheses waiting for numeric and experimental examination. This will subject of separate papers.

REFERENCES

- [1] N.I. Mezin, *Pis'ma v ZhTF* **37**, No.23, 61 (2011) (in Russian; translated to English by AIP).
- [2] N.I. Mezin, A.A. Grishchenko, and Yu.E. Kuzovlev, *Pis'ma v ZhTF* (in press).

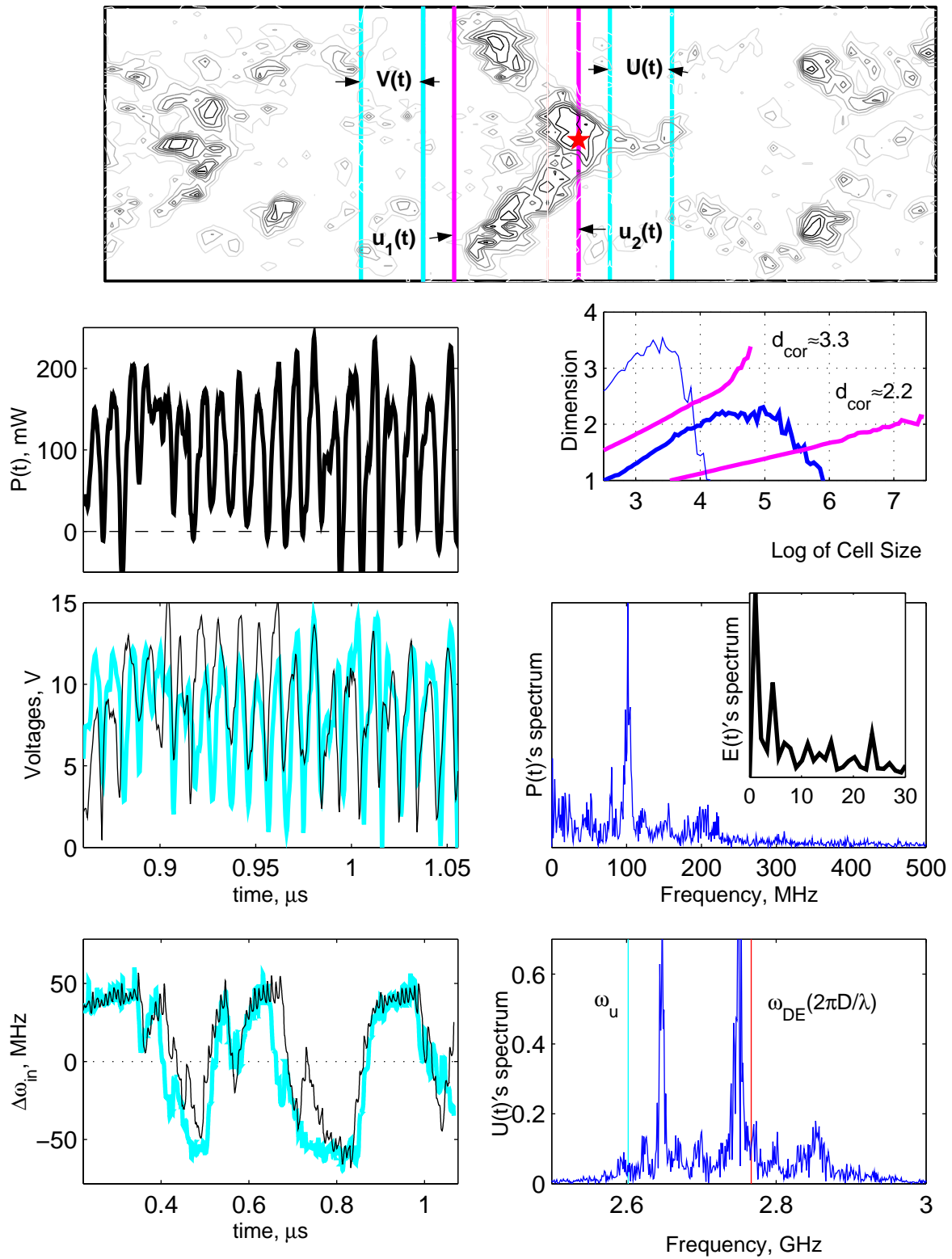


Fig.26a. Auto-generation of power absorption pulses in moderately pumped film at $H_0=400$ Oe, $\lambda=2l=0.08$ cm, $x=2\lambda$, $w/\lambda=2.5$, $\gamma=7\cdot 10^{-4}$, $I_{\text{sat}}=100$ mA, $U_{\text{sat}}=1$ V, Gain=3. (Top) Quasi-local energy pattern. (Left) Power pulsations, envelopes of feedback (thin dark) and active loop (fat light) voltages, $U(t)$ and $V(t)$, and their time-smoothed instant frequencies. (Right) Fractal dimension of energy, $E(t)$, occurs ≈ 2.2 versus that of $U(t)$ being ≈ 3.3 . Power and voltage spectra show that typical period of soliton births is ≈ 10 ns.

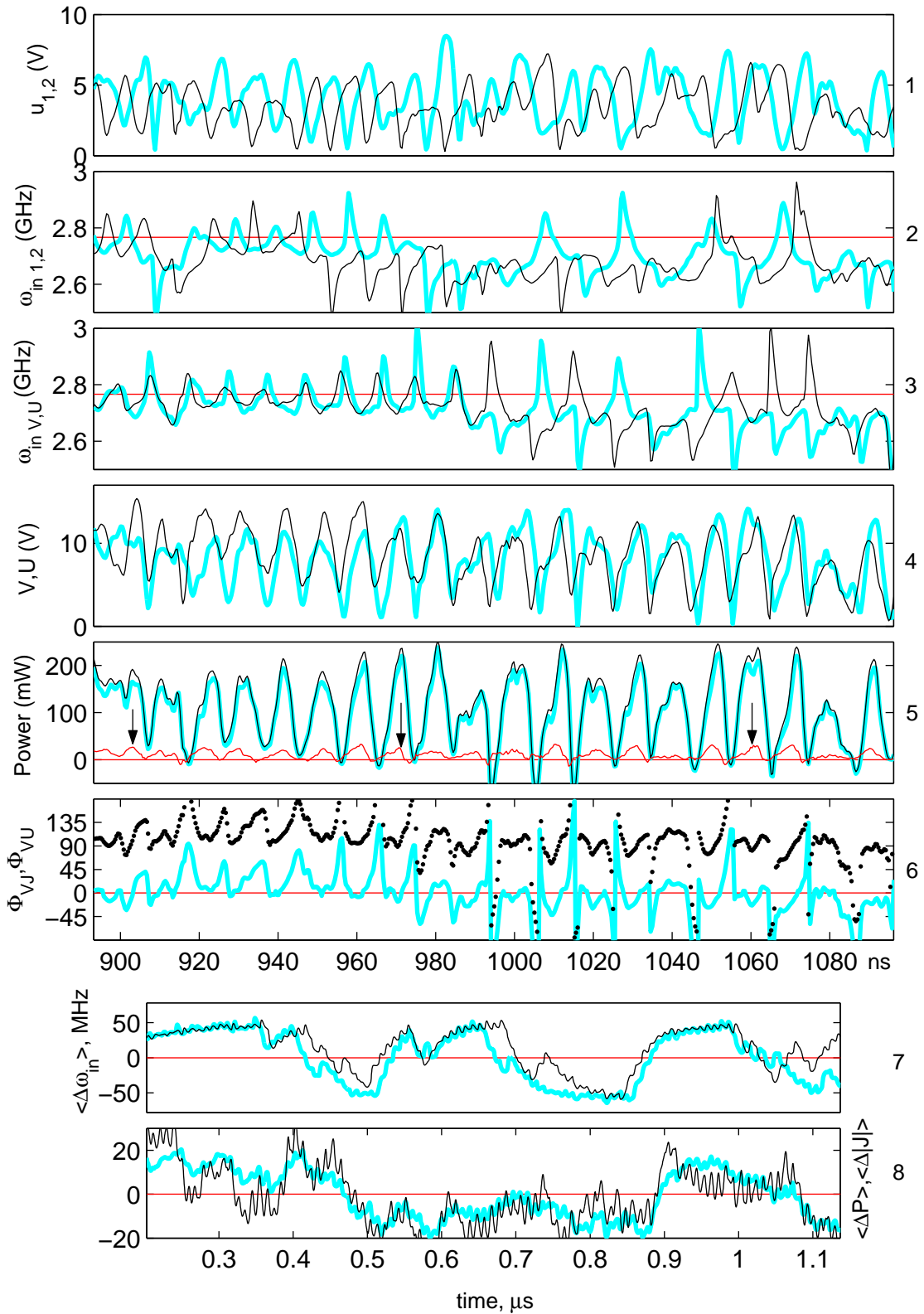


Fig.26b (continuation to Fig.26a). Dynamics of the power pulses formation. (1) Amplitudes of voltages on two control wire inductors shown at Fig.26a(A), $u_1(t)$ (fat curve) and $u_2(t)$ (thin), and (2) their instant frequencies. (3) Instant frequencies of $V(t)$ (fat) and $U(t)$ (thin), and (4) their amplitudes. (5) Power absorption (fat), $|V(t)||J(t)|\cos(\phi_V - \phi_J)$ (thin), and power consumption by feedback loop (marked by arrows). (6) Phase differences between $V(t)$ and $J(t)$ (light) and $V(t)$ and $U(t)$ (dark). (7) Slow deviations of V 's (fat) and U 's (thin) frequencies. (8) Slow variations of exciting current magnitude (fat) and power (thin).

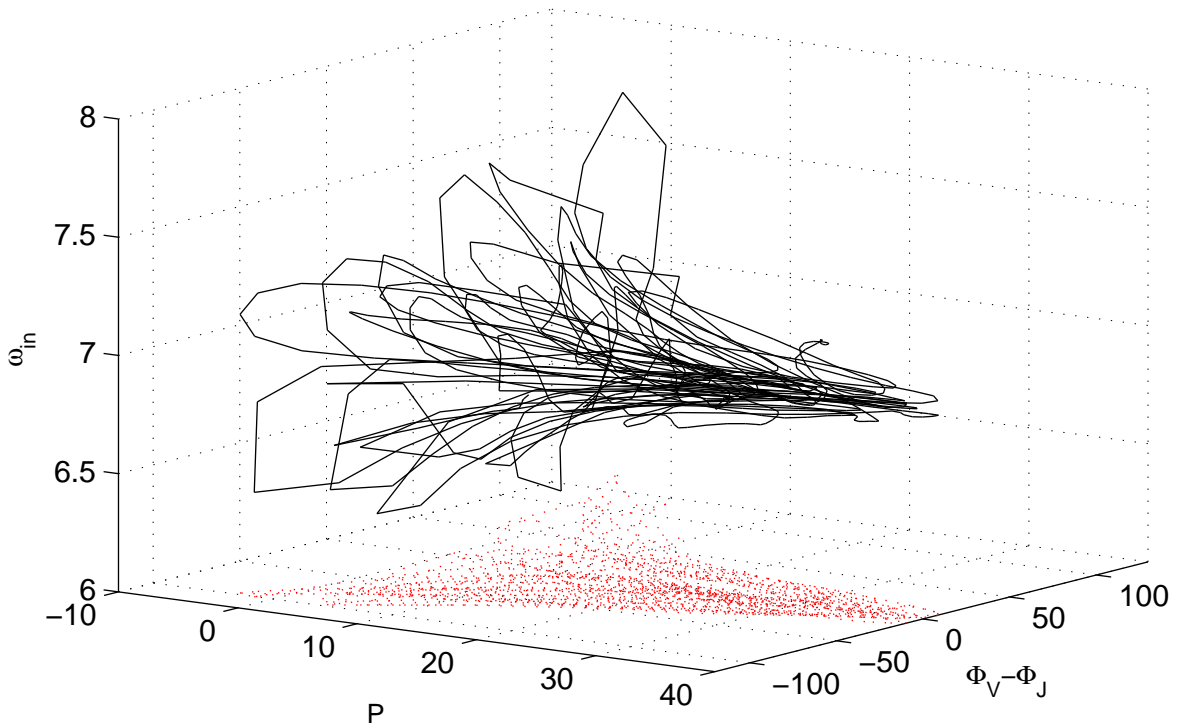
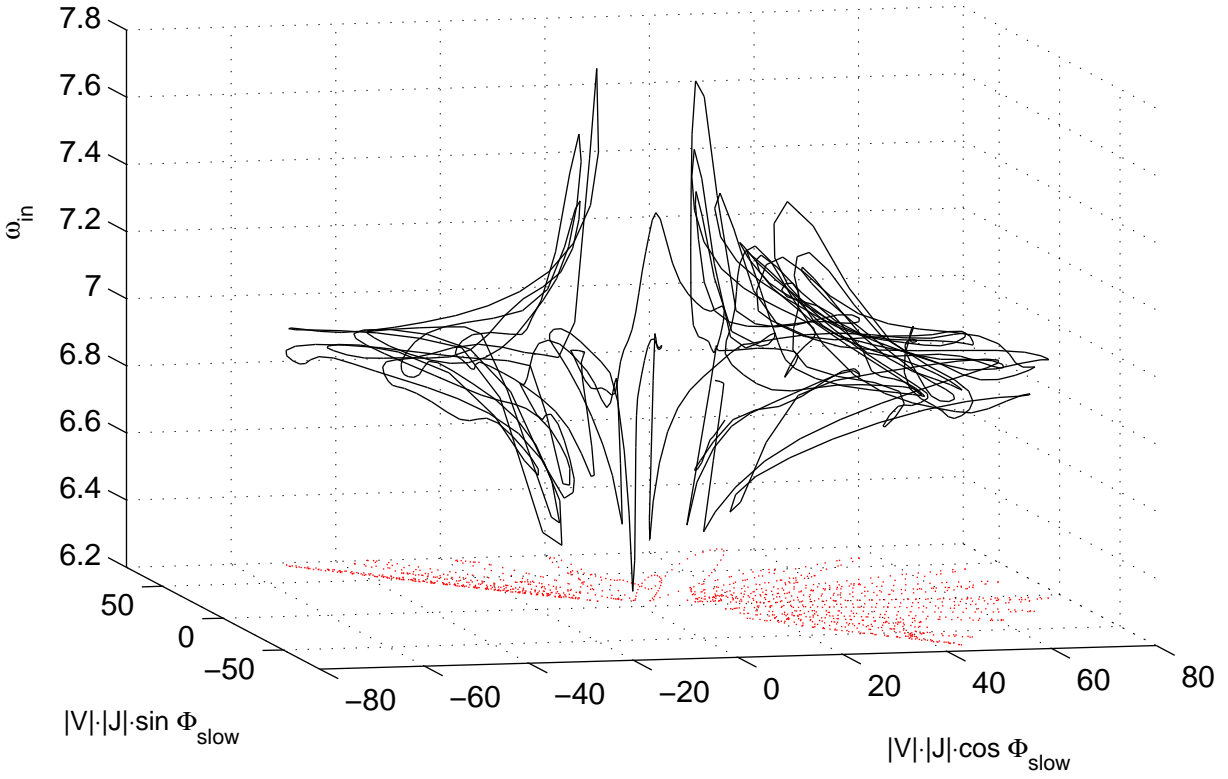


Fig.28. Two different three-dimensional representations (and their 2-D projections) of chaotic attractor of the system illustrated by Fig.26a-b. (Top) Absolute value of radius-vector in horizontal plane is chosen be product of the active loop voltage and exciting current amplitudes, $|V(t)|$ and $|J(t)|$, while its angle is scanned $\propto \Phi_{\text{slow}} \equiv \langle \omega_{\text{in}} \rangle dt$ with $\langle \omega_{\text{in}} \rangle$ being time-smoothed slow part of ω_{in} (shown at the left bottom of Fig.26a). (Bottom) Coordinates in horizontal plane are chosen be power absorption, $P(t)$, and phase difference, $\Phi_V - \Phi_J$, between $V(t)$ and $J(t)$.